University of Zurich[UZH]

Zurich Open Repository and Archive
University of Zurich
University Library
Strickhofstrasse 39
CH-8057 Zurich
www.zora.uzh.ch

Year: 2019

Comparison and contrast in soil depth evolution for steady state and stochastic erosion processes: possible implications for landslide prediction

Yu, Fang ; Hunt, Allen ; Egli, Markus ; Raab, Gerald

Abstract: The importance of gradual erosion relative to landsliding depends predominantly on the slope angle. One factor of critical influence in landsliding along with slope angle and slope shape is the soil depth. Understanding soil depth development on steep topography is fundamental for understanding and predicting the occurrence of landsliding at threshold landscapes. We develop a model to predict soil depth that addresses both threshold and gradual processes. If erosion is a gradual process, soil depth increases until the soil production rate no longer exceeds the erosion rate, and steady state is reached. The predicted soil depth (x) is proportional to the ratio of the infiltration to the erosion rate. Identifying a predictive result for erosion as a function of slope angle (S) allows a test of both the erosion and soil production models with field observations. The same theoretical approach to soil production should be applicable when the principal erosion process is shallow landsliding. After landslides, soil recovery initially follows our predicted power law increase in time, though with increasing time background erosion processes become important. At a time equal to a landslide recurrence interval, the soil depth can exceed the steady state depth by as much as a factor 2. By comparing predicted and observed x(S) results, we show that the accessed result for erosion as a function of slope angle is accurate. Soils deeper than the depth predicted at the landslide recurrence interval are beyond the stability limit. This result suggests an important practical relevance of the new soil production function.

DOI: https://doi.org/10.1029/2018gc008125

Posted at the Zurich Open Repository and Archive, University of Zurich
ZORA URL: https://doi.org/10.5167/uzh-179691
Journal Article
Accepted Version

Originally published at:
Yu, Fang; Hunt, Allen; Egli, Markus; Raab, Gerald (2019). Comparison and contrast in soil depth evolution for steady state and stochastic erosion processes: possible implications for landslide prediction. Geochemistry, Geophysics, Geosystems, 20(6):2886-2906.
DOI: https://doi.org/10.1029/2018gc008125

Comparison and contrast in soil depth evolution for steady-state and stochastic erosion processes: Possible implications for landslide prediction

Fang Yu[a]
Allen Hunt[b,c]
Markus Egli[d]
Gerald Raab[d]
[a]Department of Forestry, Beihua University, 3999 BinjiangdongRoad, Jilin, Jilin, 132013, China
[b]Department of Earth & Environmental Sciences, Wright State University, 3640 Colonel Glenn Highway, Dayton, OH 45435, USA
[c]Department of Physics, Wright State University, 3640 Colonel Glenn Highway, Dayton, OH 45435, USA
[d]Department of Geography, University of Zürich, 8057 Zürich, Switzerland

Key points:

1) Steady-state soil depth is proportional to the infiltration, but inversely proportional to the erosion rate, when erosion is gradual.
2) A quasi-universal prediction of soil depth as a function of slope angle is generated for gradual erosion and landsliding.
3) While mean slope depths for gradual erosion and landsliding are similar, for the same total erosion rate, greater depths can be achieved in the latter.

Abstract

The importance of gradual erosion relative to landsliding depends predominantly on the slope angle. One factor of critical influence in landsliding along with slope angle and slope shape is the soil depth. Understanding soil depth development on steep topography is fundamental for understanding and predicting the occurrence of landsliding at threshold landscapes. We develop a model to predict soil depth that addresses both threshold and gradual processes.

If erosion is a gradual process, soil depth increases until the soil production rate no longer exceeds the erosion rate, and steady-state is reached. The predicted soil depth (x) is proportional to the ratio of the infiltration to the erosion rate. Identifying a predictive result for erosion as a function of slope angle (S) allows a test of both the erosion and soil production models with field observations. The same theoretical approach to soil production should be applicable when the principal erosion process is shallow landsliding. After landslides, soil recovery initially follows our predicted power-law increase in time, though with increasing time background erosion processes become important. At a time equal to a landslide recurrence interval, the soil depth can exceed the steady-state depth by as much as a factor 2. By comparing predicted and observed $x(S)$ results, we show that the accessed result for erosion as a function of slope angle is accurate. Soils deeper than the depth predicted at the landslide recurrence interval are beyond the stability limit. This result suggests an important practical relevance of the new soil production function.

Keywords: soil production function, landslides, threshold slope, percolation theory

1. Introduction

Johnson & Schaetzl (2015) review two prominent competing frameworks to understand soil production that can be traced either to Darwin (1881) (bioturbation), or to Dokuchaev (1948) (soil formation factors, including e.g., climate). The former can be applied to understand particle size zonation, while the latter is amenable to derivation in terms of the limits introduced by chemical weathering (Yu *et al.,* 2017). In the latter theoretical understanding, a primary importance is assigned to vertical water fluxes in promoting the chemical weathering by bringing in weathering reagents and transporting out weathering products. Water pathways in underlying bedrock are generally recognized to be fractures, but the dominant mechanism in propagating such fractures has not been identified, as both the roles of tree roots (Gilbert, 1877; Pawlik *et al.,* 2016) and chemical weathering (Eppes & Keanini, 2017) have been established. In any case, quantifying the production and erosion of soil is key in a wide range of agricultural (Blanco and Lal, 2010; Montgomery, 2007a), cultural history (Montgomery, 2007b), geomorphological (Gilbert, 1877; Heimsath *et al.,* 1997), and climatic studies (Kump *et al.,* 2000), including elemental cycling (Hartmann *et al.,* 2014).

The constraint placed on chemical weathering from solute transport is a phenomenon that is receiving increased attention as possibly the most important limitation on soil production (Burke *et al.,* 2006,2009; *Dixon et al.,* 2009ab; Anderson & Anderson, 2010; Maher, 2010; Egli *et al.,* 2014). Hunt et al. (2016) recently developed the theoretical framework for modelling soil production and chemical weathering based on solute transport limitations. It has, in common with other commonly used soil production models (e.g., the exponential phenomenology of Heimsath *et al.,* 1997), the feature that soil production diminishes with increasing

depth. However, it differs from the exponential phenomenology in that its spatial dependence is a power-law, making the temporal evolution also a power-law, in accord with observed chemical weathering rates (e.g., White & Brantley, 2003). Moreover, the parameters of the function have direct physical origins traceable to the values of vertical water fluxes and typical particle sizes (e.g., Yu *et al.,* 2017). Further, it is in accord with a century of the theory of soil development (Yu *et al.,* 2017), from Dokuchaev (1948) onwards (translation 1948, original from 1883).

The derived soil production rate is proportional to the infiltration (water) flux, I. The power-law function of time and proportionality to infiltration have direct implications for the question of whether landscapes are in steady-state; there is neither implicit assumption of a maximum, or limiting soil depth, nor is there an identification of a maximum in soil production in the limit of vanishing soil thickness, although the theoretical bounds on the applicability of the theory place practical limitations in soil production. Further, the result for the steady-state soil thickness is proportional to $(I/D)^{1.15}$, with D the denudation rate. Such a power-law can be contrasted with other formulations available in the literature (Heimsath *et al.,* 1997, 1999; Roering, 2008), which, due to the assumed exponential dependence of soil production on depth, generate logarithmic functions of depth on soil production and thus erosion. One reason given to provide understanding for an exponential form for the depth dependence of soil production is the concept of soil development through bioturbation (Huntly & Inouye, 1988; Yoo *et al.,* 2005). Bioturbation models can be applied effectively to explain layering in particle sizes (Johnson & Schaetzl, 2015 and references therein).

The emphasis here is on predicting specific values of the soil depth as a function of erosion rate based on a local condition of steady-state. It is not on the specific hillslope form developed or on the surface transport properties of the system. We will take the erosion rate, for example, as an input parameter without constraining its values from point-to-point by the conservation of surface sediment flux. Heimsath et

al. (1999) argue that use of the diffusion equation for surface sediment transport leads to steady-state values of the soil production rate which are proportional to the negative of the landscape curvature, i.e., higher on ridgetops where soil is eroded, and lower in hollows. Here, a result with practical similarities is obtained from a soil production function which is linearly proportional to the infiltration water flux. Since, when not limited by bedrock hydraulic conductivity values, infiltration will typically be higher in hollows and lower on ridgetops (Dunne et al., 1991), soil depths will adjust to be lower on ridgetops in order to tend towards a spatially uniform soil production and denudation rate. This argument depends on surface water routing, thus on regolith, or soil, hydraulic conductivity values compared with rainfall and transpiration rates, although the bedrock hydraulic conductivity on ridgetops may be higher than in valleys (St. Clair et al. 2015).

In summary, the curvature of a hill promotes a similar spatial variability in soil depth in both the exponential model and in ours; directly in our case, due to the variation in infiltration, while in the case of Heimsath et al. (1999) it is a result of the adjustment of the production rate to the erosion rate under the assumption of steady-state evolution at the landscape level. This distinction appears to make our results for soil production and soil depth relevant to different locations in a given watershed, as well as to different watersheds with distinct climates. The strong climatic dependence of soil production function parameters, e.g., infiltration rate, and the power-law dependence of the soil depth on erosion rate (rather than the more typical logarithmic phenomenology) also suggest that there may be important implications for the evolution of steep topography with strongly variable precipitation and erosion rates.

Studies of steep topography are of continuing interest in geomorphology. The morphologic characteristics of landscapes reflect the complex feedback between tectonics and climate-driven processes in sculpting the topography. Tectonically active landscapes are often exposed to natural hazards, such as landslides, debris

136 flows, floods and earthquakes. These phenomena typify threshold processes that
137 generate significant impacts on topography. Unresolved questions about threshold
138 landscapes range from the conceptual (DiBiase *et al.,* 2012), such as whether such
139 landscapes respond obviously and meaningfully to changes in erosion rates, to the
140 practical (e.g., Montgomery & Brandon, 2002), such as how to predict such erosion
141 rates. What constitutes steady-state in a threshold landscape? Several worldwide
142 studies demonstrate an equivalence between soil production and soil erosion. In a
143 threshold landscape, such an equivalence can only reflect a spatial, or long-term
144 average. The relevance of steady-state landscapes has been called into question
145 (Phillips, 2010; Yu & Hunt, 2017a), even though an equivalence of soil production and
146 soil erosion rates is often assumed. Nevertheless, the investigation of Yu and Hunt
147 (2017a) indicated that, while slowly evolving landscapes in arid continental interiors
148 were unlikely to be in steady-state, tectonically active regions were much more likely
149 to conform to steady-state conditions, at least if erosion processes were largely
150 gradual. The same conclusion was reached in a study of Braun et al. (2016).
151 Many studies have addressed quantitative understanding of the relationship
152 between erosion rate and topographic elements including hillslope gradient,
153 topographic relief, hilltop curvature, and drainage density (e.g., Gilbert, 1877; Ahnert,
154 1970; Montgomery & Brandon, 2002; Binnie *et al.,* 2007; Roering, 2008; DiBiase *et*
155 *al*., 2010; Hurst *et al.,* 2012; DiBiase *et al.,* 2012). General conclusions, however,
156 have been slow to develop.
157 Ahnert (1970) reported a linear relation between erosion rate and mean local
158 relief at mid-latitude drainage basins. However, several studies have demonstrated
159 that the linear relationship breaks down as the mean slope increases and approaches
160 a threshold angle of stability S_c (e.g., Carson & Petley, 1970; Schmidt & Montgomery,
161 1995; Ouimet *et al.,* 2009; Montgomery and Brandon, 2002; Binnie *et al.,* 2007;
162 DiBiase *et al.,* 2010), at which downslope sediment fluxes can become infinite
163 (Roering *et al.,* 2007). In this case, sediment flux switches from creep-related process

164 to mass wasting (DiBiase *et al.,* 2012), and landslides can occur, such that hillslope
165 lowering prevents the hillslope from becoming steeper than S_c, and erosion rate and
166 topographic relief become decoupled (Schmidt & Montgomery, 1995; Burbank *et al.,*
167 1996; Montgomery, 2001; Montgomery & Brandon, 2002). The fundamental
168 characteristics of the empirical erosion formula given by these last authors
169 incorporates effects from both gradual erosion and landsliding and will be applied in
170 the modeling here.

171 Accurate modelling of landsliding processes is relevant not only to a general
172 understanding of geomorphology, but also to prediction and diagnosis of landsliding
173 hazards. According to Claessens et al. (2007) “High annual rainfall, steep slopes,
174 deforestation, high weathering rates and slope material with a low shear strength or
175 high clay content are considered the preparatory causal factors for mass
176 movements.” In order to make predictions of when such landsliding may be imminent,
177 one must also take into account the moisture history of slopes, modelling the spatial
178 distribution of moisture, pore pressure, and soil strength (Dietrich *et al.,* 1995),
179 addressing Coulomb failure and friction forces (Dietrich *et al.,* 2007), and many
180 combinations thereof (Claessens *et al.,* 2007).

181 Nevertheless, soil depth is often considered (Okimura, 1987; Iida, 1999) to be the
182 most important parameter for predicting a general risk of shallow landsliding. Thus,
183 understanding soil depth development on steep topography may be useful for
184 understanding and predicting the frequency of occurrence of landsliding in threshold
185 landscapes. But modeling threshold processes, let alone landscapes, holds additional
186 theoretical and practical challenges.

187 Up to the present, our theoretical development has addressed only the evolution
188 of soil depth for gradual erosion processes. In order to broaden the investigation, we
189 now also investigate theoretically mean soil depths between landslides in threshold
190 landscapes. Here it is shown that, for our power-law dependence on soil depth of the
191 soil production function (SPR), the mean soil depth is given by an analytical result

192 almost identical to that for the steady-state soil depth for gradual erosion. Thus, for the
193 same erosion rate, the predicted mean soil depth is scarcely dependent on whether
194 the erosion is by gradual or threshold processes. Therefore, we propose to predict
195 mean soil depths in both landslide-dominated landscapes and landscapes dominated
196 by gradual erosion processes such as soil creep, as long as one has specific
197 evidence for the magnitude of the relevant erosion processes. In any case, soil depth
198 clearly varies with hillslope gradient. Thus one requires either suitable measurements
199 of erosion rates, or an accurate model of erosion rate with hillslope gradient. For the
200 latter situation we adopted the phenomenology proposed by Montgomery & Brandon
201 (2002) (MB).
202 Influences of climate, parent material, relief, and time also vary from place to
203 place. Consequently, the soil production function (SPR) must be evaluated at
204 individual sites using either existing parameters, or alternatively, the best guidance for
205 generating such parameters from published information.
206 Using climate, soil texture, and erosion data from the San Gabriel Mountains
207 (SGM) in California, USA, we parametrize the MB slope-dependent erosion rate
208 function and then compare predictions of the slope-angle dependence of soil depth
209 and soil production with field results for soil production functions and soil depth. Such
210 investigations are then repeated at other sites, even though typically less information
211 was available for verification purposes. For the SGM, these tests also utilize
212 exponential SPR formulations for comparison. We also investigate the validity of our
213 proposed SPR and its predictions for soil depths as a function of time on slopes
214 recovering from landslides.
215 Should the proposed SPR be assessed to be useful, its implications for regional
216 and local variability in soil production may help solve related questions in
217 geomorphology, such as whether soil transport is linear (Heimsath et al. 2005), or
218 how to predict regional denudation rates, both under past climates and for future
219 scenarios.

Finally, we discuss the potential relevance of our prediction for the SPR to landslide risk assessment. Here, the focus is not to evaluate spatial variability in stochastic triggers, such as rainstorms, fires, or land-use changes, in development of real-time landslide risk assessment. But, if it proves possible to generate guidance on which slopes may exhibit elevated risk for landsliding based on their depths and the slope angle, this will be a useful advance in itself.

2. General Model

We describe initially some theoretical extremes before combining them into a single, more generally applicable, model. The first is a soil production model without erosion. Then erosion is added, initially as an exclusively gradual process, later as a stochastic process representing a catastrophic (threshold) phenomenon of total soil loss by landsliding. In these tests, the analytical result of Montgomery and Brandon (2002) is applied. In each case, the soil production model remains the same, however, and we start with that input.

2.1. Soil Production Models

The present discussion will focus on the percolation model applied here as well as contrast it with a related power-law model of soil production. It will also provide sufficient detail to understand subtleties in the exponential soil production model.

Percolation Model

Our model for soil formation derives from solute transport theory in porous media (Hunt & Skinner, 2008) developed from percolation theory. For a recent review on applying percolation theory, PT, to solute transport, chemical weathering and soil formation, see Hunt & Sahimi (2017). Within the framework of PT, solute velocity

diminishes with increasing solute transport distance in porous media, and the scaling of travel time (t) on travel distance (x) is determined by the fractional dimensionality of the percolation backbone (D_b), $t \propto x^{D_b}$. Here, D_b = 1.87, for 3D media under conditions of full saturation (Sheppard *et al.,* 1999), and is nearly the same, 1.861 under wetting conditions. If most downward solute transport occurs during wetting or under saturated conditions, then it is reasonable to use D_b = 1.87 generally.

This scaling result from PT is argued (Sahimi, 1994) to be generally applicable to solute transport in disordered porous media on account of the tendency for flow to be concentrated along tortuous paths formed from the least resistive elements of the medium. Such paths can, in principle, be identified using the critical percolation probability, and their tortuosity is described by a fractal dimension, rather than a constant factor. Because chemical weathering in the field is indicated to be solute transport-limited (Yu & Hunt 2017b), as anticipated by Maher (2010), close correlation of chemical weathering rates with soil production rates (Hunt & Ghanbarian, 2016; Egli *et al.,* 2012, 2014) makes it possible to relate soil transport distances and soil depths. Thus, in the absence of erosion,

$$x = x_0 \left(\frac{t}{t_0}\right)^{1/D_b} = x_0 \left(\frac{t}{t_0}\right)^{1/1.87} \qquad \text{Eq. (1)}$$

describes the evolution of soil depth x as a function of time t by using the scaling properties of solute transport in disordered networks. In Eq. (1), the length scale, x_0, and time scale, t_0, are required by dimensional analysis, but these constants have physical relevance, and are connected to the fundamental structure of a porous medium as a network. Consequently, x_0 is identified (Yu *et al.,* 2017) as a typical particle size, for which we substitute d_{50}, the median value. t_0 is the typical pore crossing time under fluid flow at a characteristic pore-scale flow rate, v_0.

By taking the derivative of soil depth, one can derive the equation for soil production (equivalent to a solute, or weathering front, velocity) (R_s),

$$\frac{dx}{dt} = R_s = \frac{1}{1.87}\frac{x_0}{t_0}\left(\frac{t}{t_0}\right)^{-0.47} = \frac{1}{1.87}\frac{I}{\phi}\left(\frac{x}{x_0}\right)^{-0.87} \qquad \textit{Eq. (2)}$$

Here, $\frac{I}{\phi} \equiv x_0/t_0$ is the pore-scale vertical flow rate at the bottom of the soil column (Yu *et al.,* 2017), i.e., net (deep) infiltration rate *I* with porosity ϕ, and *I* = Precipitation (*P*) - Actual Evapotranspiration (*AET*) + *run-on* - *run-off* by overland flow (Hunt & Ghanbarian, 2016). It should be kept in mind that even though the pore-scale constants in Eq. (2) relate geologic time and space scales to pore-scale processes, Eq. (2) only becomes limiting for soil formation rates at time and spatial scales for which the product of Eq. (2) and the molar density of the principle reaction products is less than the initial reaction rate from reaction kinetics (Yu & Hunt, 2017b). Where this occurs varies, ranging apparently from length scales less than a millimeter (Maher, 2010; Yu & Hunt, 2017b; Egli et al. 2018) up to centimeters (Egli et al. 2018).

Exponential Model

The power-law soil production function in Eq. (2) contrasts with the exponential model of Heimsath et al. (1997; 2012), where *R* (which corresponds to *dx*/*dt* in Eq. (2)) = R_0 exp (-x/x_s). Here x_s is typically about 0.5m, *x* is the thickness of soil, and R_0 is a maximum soil production rate, obtained from extrapolation of experimental soil production data to zero soil thickness. In usual applications, steady state conditions are invoked to equate *R* with a denudation rate, *D*, yielding a soil depth. Inversion of the resulting exponential relationship $D = R_0\exp(-x/x_s)$ yields,

$$x = x_s ln\left(\frac{R_0}{D}\right) \qquad \textit{Eq. (3)}$$

301 Except when D is very near R_0, this logarithmic relationship is insensitive to R_0 and D,
302 and it is highly unusual for x to greatly exceed x_s, in accord with the global tendency
303 for soil depths (Hillel, 2005) to be on the order of 1m.
304
305 *Related Model (Braun et al. 2016)*
306
307 The model of Braun et al. (2016) yields chemical weathering and soil formation
308 proportional to flow rates, as well as to soil depth to a power of time similar to ours.
309 The work couples hillslope evolution models with water table evolution in time, but
310 uses zero hydraulic conductivity for bedrock and assumes initial conditions of full
311 saturation over the entire slope. Their result for regolith thickness, x, at the bottom of a
312 hillslope is $x = ((LP/K_hS)^2+2FPLt)^{1/2}$, with L slope length, K_h (m yr^{-1}) the hydraulic
313 conductivity, F a dimensionless parameter proportional to the weathering reaction
314 rate, P the precipitation (m yr^{-1}) S (dimensionless) the slope gradient and t (yr) the
315 time elapsed since the entire hillslope becomes unsaturated. In contrast, field
316 experiments exhibit a stronger dependence of regolith thickness on reaction rate at
317 shorter than at longer times (Hunt & Ghanbarian, 2016; Egli *et al.,* 2018), while a
318 regolith thickness inversely proportional to K_h at early times is not consistent with the
319 result that higher infiltration rates produce higher soil formation rates.
320 Harman *et al.,* (2017) argue that an inconsistency in the approach leads to a
321 concentration of weathering products at the bottom of the slope much larger than the
322 equilibrium value. Harman et al. (2017) attribute the discrepancy to inconsistent
323 treatment of the dimensionality of flow. However, Braun et al. (2017) assert that any
324 discrepancy is removed if one does not assume that the reaction products in solution
325 are in equilibrium, similar to our understanding.
326 The square-root dependence of soil depth on duration of unsaturated conditions
327 recalls Philip (1957; 1967) infiltration theory for the infiltration depth; preserving even
328 the dependence on the square root of K_h (Hunt *et al.,* 2017). The inference of the

329 importance of unsaturated conditions, however, precludes using the Braun et al.
330 (2016) model for weathering experiments in (1D) columns under saturated conditions
331 (Salehikhoo *et al.,* 2013; White & Brantley, 2003), but which produce the same
332 proportionality to flow rate and the same time-dependence of weathering rates as do
333 field experiments. In contrast, our soil formation and chemical weathering model is
334 applicable in both lab (Hunt *et al.,* 2015) and field settings (Hunt *et al.,* 2014; Hunt &
335 Ghanbarian, 2017), and under either saturated or unsaturated conditions.
336
337 **2.2. Causes of Soil or Regolith Loss**
338
339 The mantle of soil can form in unconsolidated material, such as alluvium,
340 landslide deposits, mining tailings, etc., or from bedrock. Erosion of such
341 unconsolidated material is occurring constantly through physical and chemical
342 processes. For example, chemical weathering products are partly soluble and for
343 some substrates, such as carbonates, removal of mass in solution is particularly
344 important. Thus, it is advisable to consider both chemical and physical agents for loss
345 of mass from the surface, and define a total denudation rate, $D(t)$, which can, in
346 principle, depend on time.
347
348 **2.3 Gradual Erosion Treatment**
349
350 When a time-dependent denudation rate, $D(t)$, is included, one can now obtain the
351 net formation rate of soil, equal to the time derivative of its depth,
352
353 $$\frac{dx}{dt} = R_s - D(t) = \frac{1}{1.87}\frac{I}{\phi}\left(\frac{x}{x_0}\right)^{-0.87} - D(t) \qquad \textit{Eq. (4)}$$
354
355 Physical soil erosion is chiefly accomplished through advective processes such as
356 overland flow and rainsplash (Anderson & Anderson, 2010). The erosion rate at a

given site relates to various factors including climate, particle size and local variations in slope and curvature, as well as total relief (Montgomery & Brandon, 2002; von Blanckenburg 2005). It can vary over about 4 orders of magnitude, from less than a meter per million years in the interior of Australia (Bierman & Nichols, 2004) or the Atacama Desert (Owen *et al.,* 2010) to over 1000 meters per million years in the Himalaya (Bierman & Nichols, 2004) or New Zealand Alps (Larsen *et al.,* 2014). In the simplest case, $D(t)$ is treated as time-independent, D, although clearly such climate change as occurred at the beginning of the Holocene produced detectable changes in landscape characteristics in many locations worldwide.

D is often broken down into slope-independent, E_0 and slope-dependent terms, KS, where K is a constant of proportionality, and S is the slope angle. E_0 is then usually conceptualized as a loss of soil volume due to the removal of soil products by chemical weathering, which may also be time-dependent, since, as long as steady-state is not reached, chemical weathering and soil production are time-dependent. The term with linear dependence on slope is consistent with a steady-state solution of topography where soil production is proportional to the (negative) of the landscape curvature (e.g., Heimsath *et al.,* 1999). This result is then coupled with the inference (Heimsath et al., 1999) that soil production on the top of hills is greater than that at the bottom, with an associated lateral transport of soil from the top to the bottom. For steeper slopes and threshold topographies, more complicated forms of erosion rates from physical processes, including a dependence on depth, may be considered (Roering, 2008). Whatever the particular form of the slope dependence, whenever the long-term erosion rate can be considered time-independent ($D(t) = D$), Eq. (4) becomes,

$$\frac{dx}{dt} = R_s - D = \frac{1}{1.87}\frac{I}{\phi}\left(\frac{x}{x_0}\right)^{1-D_b} - D \qquad \textit{Eq. (5)}$$

As long as $R_s \neq D$, $\frac{dx}{dt} \neq 0$, i.e., the soil thickness changes. If initially, $R_s > D$ ($R_s < D$) the soil progressively deepens (thins) until $R_s = D$. At this point $\frac{dx}{dt} = 0$ and steady-state is reached. Setting $\frac{dx}{dt} = 0$ yields for the steady-state soil depth, x_{ss},

$$x_{ss} = x_0 \left(\frac{1}{1.87}\frac{I}{\phi D}\right)^{1/(D_b-1)} = x_0 \left(\frac{1}{1.87}\frac{I}{\phi D}\right)^{1.15} \qquad \textit{Eq. (6)}$$

Here the combination of exponents (1/(D_b -1)) yields the power 1.15. Thus, with the knowledge of relations between a steady-state denudation rate, D(S) as a function of mean slope angle, *S*, plus reliable estimations of the parameters x_0 and *I*, Eq. (6) can be used to predict $x_{ss}(S)$.

Further, if erosion is purely a gradual process, soil depth at any age can be predicted from the integration of Eq. (5),

$$x = \int_0^t dt' \, (R_s - D) = \int_0^t \left(\frac{1}{1.87}\frac{I}{\phi}\left(\frac{x(t')}{x_0}\right)^{-0.87} - D\right) dt' \qquad \textit{Eq. (7)}$$

2.4. Threshold Process Modelling

Where landslides dominate the erosion, the purely gradual approach is not valid. Consider first how to address a problem in which gradual processes are, in some fashion, small enough to be negligible in order to understand the overall effects of threshold erosion processes. Although we consider this distinction in greater detail in Section 4, an initial assessment can be based on the magnitude of the contribution of landslides to the total denudation rate compared with that due to gradual processes. If the former is much larger than the latter, to first approximation, the gradual processes can be neglected. When the gradual contribution to the denudation rates is small, one can ask how the effects of an unsteady erosion rate would contribute to the mean soil development. This can be found by using the power-law soil depth equation to relate

411 t_l, a typical time between landslides, and x_l a typical soil depth at which landslides
412 occurs. Then $x_l/t_l = D$. Neglecting gradual erosion processes, we have
413
414 $$x_l = x_0 \left(\frac{t_l}{t_0}\right)^{\frac{1}{D_b}} = x_0 \left(\frac{x_l/D}{\phi x_0/I}\right)^{\frac{1}{D_b}} \qquad \textit{Eq. (8)}$$
415
416 Straightforward algebraic solution of Eq. (8) yields
417
418 $$x_l = x_o \left(\frac{I}{\phi D}\right)^{\frac{1}{D_b - 1}} = x_o \left(\frac{I}{\phi D}\right)^{1.15} \qquad \textit{Eq. (9)}$$
419
420 The only difference between the result of Eq. (9) and that of Eq. (6) is the absence of
421 the factor $1.87^{-1.15}$, an effective increase in soil depth by a factor 2.05. Calling this a
422 factor 2, Eq. (8) would imply that when the majority of erosion occurs by landsliding,
423 the maximum soil depth that is typically reached before a landslide occurs is twice the
424 depth that would be attained if the same erosion rate were developed in a steady
425 process. But the apparent contrast with gradual erosion processes is reduced, if one
426 considers the temporal mean soil depth. An average depth over the time interval $0 < t$
427 $< t_l$ is t_l^{-1} $(t_l^{1.53}/(1.53))$, or $(1/1.53)$ $t_l^{0.53}$, meaning that use of Eq. (6) to predict an
428 average depth, instead of the final depth, would require substitution of (0.65) $t_l^{0.53}$ for t_l
429 $^{0.53}$. A numerical factor 0.65, is not so different from the factor $1/D_b = 0.53$. We assume
430 that the mean soil depth over similar slopes in a specific geographical region
431 characterized by an unsteady, but mean, denudation rate D, will be the same as the
432 temporal mean calculated above.
433 Thus, in both Eq. (6) and Eq. (9), the functional dependence of the soil depth on
434 D, I, and x_0 is the same. If landsliding is the dominant erosion process, for the same
435 combination of parameters, the result from Eq. (6) gives a good estimate of the mean
436 soil depth, while the result from Eq. (9) would give a maximum soil depth. Further, a
437 good approximation to the mean slope depth can, for all slope angles, be found by
438 substituting a single result for D into Eq. (6) that combines effects of both gradual and

439 threshold erosion, even if the relative importance of landsliding increases with the
440 slope angle. Then, where landsliding is dominant, Eq. (9) should give the maximum
441 soil depth. However, if landsliding is not a relevant process at low slope angles, Eq.
442 (9) will tend to overestimate maximum soil depths.
443 In the case that erosion is predominantly by landsliding, the exponential
444 phenomenology, Eq. (3) yields a result that is not strictly defensible, since, until a
445 landslide occurs, the erosion rate can be considered negligible. Since cases with
446 mixed erosion sources are more difficult to deal with analytically, we address the case
447 of erosion solely by landsliding. Then one has
448
449 $$R \equiv \frac{dx}{dt} = R_0 exp\left(-\frac{x}{x_0}\right) \qquad \textit{Eq. (10)}$$
450
451 Eq. (10) may be integrated to generate
452
453 $$x = x_0 ln\left(\frac{R_0 t}{x_0}\right) \qquad \textit{Eq. (11)}$$
454
455 If all erosion is by landsliding, one can also set x/t equal to the denudation rate. Then
456 one finds
457
458 $$\frac{Dt}{x_0} = ln\left(\frac{R_0 t}{x_0}\right) \qquad \textit{Eq. (12)}$$
459
460 Transcendental equations such as Eq. (12) cannot be solved exactly. Moreover, it
461 turns out that for any specific value of R_0, Eq. (12) can only be solved for a restricted
462 range of parameters D. In particular, D cannot exceed R_0/e; otherwise no solutions
463 exist. For $D = R_0/e$, there is one solution, namely $Dt/x_0 = 1$, and for smaller values of
464 D, there are two solutions. The solution with the smaller depth appears to be
465 unphysical, as it yields an increasing soil depth with increasing erosion rate. If only the

second solution is considered, it will become apparent that the distinction between the solutions of Eq. (3) and Eq. (12) is not large, at least in the range of values for which Eq. (12) has a viable solution. Thus, it may be reasonable to use Eq. (3) for the entire range of observed erosion rates. One peculiarity of this approach is, however, apparent. For the stochastic solution in the exponential phenomenology, it may be necessary to distinguish between maximum denudation rates on steeper, landslide dominated, slopes and the maximum value of the denudation rates on shallower slopes without landsliding, since use of the smaller maximum *D* does not admit real solutions for soil depths on the steeper slopes. In the percolation formulation (Eq. (8)), with algebraic solution Eq. (9), there is no restriction on *D*, and the solution is valid at any slope angle.

2.5. Slope-Dependent Model of the Erosion Rate

The basic relationship between long-term erosion rate, *D*, and the mean slope, *S*, that we adopted to predict the dependence of soil depth on slope angle, combines a range of erosion effects. The empirical equation published in Montgomery & Brandon (2002, equation 1) (MB equation), was developed specifically for *D*(*S*), in the Olympic Mountains, Washington State, USA. We reprint it here as our Eq. (13) and refer to this model as the MB model.

$$\mathrm{D}(S) = \mathrm{E}_0 + \frac{\mathrm{KS}}{\left[1-\left(\frac{\mathrm{S}}{\mathrm{S_c}}\right)^2\right]} \qquad \text{Eq. (13)}$$

Relevant site-specific parameters that determine the value of *D* predicted in Eq. (13) include a constant erosion rate considered to be due to chemical weathering (E_0), a rate constant for a background physical sediment transport coefficient (*K*), and a threshold slope gradient (S_c). *S* is the slope angle. This empirical result assumes a form, *KS*, for the background sediment transport appropriate for smaller slopes that is

494 proportional to the slope as suggested by Ahnert (1970) and supported by data
495 collected by Pazzaglia & Brandon (1996). The factor in the denominator approaches
496 zero rapidly as the critical slope, S_c, is approached, producing an erosion rate that
497 tends to diverge, but whose effect on D at smaller slopes is reduced by squaring the
498 ratio of S/S_c. Eq. (13) was tested in the Olympic Mountains of the state of Washington,
499 USA, and found to yield a reasonable dependence of erosion on slope angle. It is
500 quite likely to have a wider applicability, though again only approximate, as it is
501 possible to vary the parameter S_c according to observations of the maximum soil
502 mantled slope angles in any region. The more difficult parameter to generate
503 accurately is probably K, since its variability with climate, substrate, and vegetation
504 cover is likely still too difficult to predict without extensive site-specific observations
505 and modelling.
506 Substituting Eq. (13) into Eq. (6) yields,
507

508 $$x = x_0 \left\{ \frac{I}{1.87 * \phi * \left(E_0 + \frac{KS}{1 - \left(\frac{S}{S_c}\right)^2} \right)} \right\}^{1.15} \qquad \text{Eq. (14)}$$

509
510 In the development of Eq. (14) it was assumed that each input to the denudation rate,
511 D, is independent of time. Eq. (14) displays high sensitivity to parameters such as I,
512 x_0, and the total denudation rate, D, with the uncertainty in the predicted depth equal
513 or greater than the uncertainty in these parameters. These latter uncertainties will turn
514 out to be as large as a factor 2.
515
516 **3. Materials and Methods**
517
518 **3.1 Parameter Choices and Uncertainties, Testing Strategies**
519

520 We compared predictions for soil depth and soil production as function of slope
521 angle with data from sites with distinct climates. Information to generate parameters
522 needed is incomplete, necessitating development of strategies for data collection.
523 Since the exponential phenomenology lacks the specific inputs into soil
524 production, its use is more fundamentally restricted to steady-state conditions, in
525 which soil production and soil erosion rates are assumed equal.
526 For testing the soil production model in the case of initial soil recovery following a
527 landslide, it may be sufficient to generate those constants relevant to soil production,
528 i.e., infiltration rates and particle sizes. For testing steady-state or mean soil depths,
529 some characterization of the erosion rate is necessary. In the comparison of theory
530 with field data, we have found a variety of sites, which allow more limited
531 comparisons, but only one site, the SGM, for which it is possible to test independently
532 Eq. (13) for soil erosion, as well as Eq. (14) for the soil depth as a function of erosion
533 rate. This places the comparison with field data for the SGM at the forefront.
534 In the form of Eq. (14) our prediction for the soil depth as a function of slope angle
535 has altogether 6 physical parameters: x_0, which we have assumed (e.g., Yu *et al.,*
536 2017) to be a median particle size, d_{50}, I, which is given as the deep infiltration rate, ϕ,
537 the soil porosity, E_0, a background erosion rate due to chemical weathering, which
538 takes into account mass lost in solution, K, the constant of proportionality in a linear
539 dependence of erosion on a slope gradient, and S_c, a critical slope angle. For soil
540 production data, what general guidance is available to find, e.g., I, the local infiltration
541 rate? I depends not only on climatic variables, but also on surface water routing.
542 Although progress is being made in specific catchments (Gu et al., 2018), the only
543 useful indication of how to take such run-on and run-off into account on our specific
544 sites is found in global and continental estimates (e.g., Lvovitch, 1973). In particular,
545 Lvovitch (1973) cites the global proportionality, $I = 0.23\ P$, with about a 50% variability
546 in the numerical prefactor.

Since the only information directly relevant to particle sizes that is usually available is soil texture, we had to appeal to studies that relate soil texture to median particle size (Skaggs *et al.,* 2001). The range of soil types considered is appropriate for agricultural purposes. Information for porosity was also not generally available, but since its variability is usually limited to a factor 2, i.e., from a value of about 0.3 to 0.6, variations for the porosity were not explicitly considered, unless they could be determined from alternate sources. Soil depth from the model (Eq. (14)) is proportional to particle size, and is nearly proportional to infiltration rate (to the power of 1.15). Since soil particle size can range over many orders of magnitude, but in the field studies considered the variation in infiltration rate was typically no more than about a factor 5, our model so far reflects greater variability in prediction from soil type (or d_{50}) than infiltration rate.

How does one select values of the erosion parameters that are either 1) site-specific, or 2) approximately applicable for sites where no data is available? Overall, we found no general information to help us determine either E_0 or K. On the other hand, consider S_c. In the Olympic Mountains, soil is only sustained from shallow landsliding at slope angles below 25º (Montgomery & Brandon, 2002), even though the threshold angle is stated to be 40º. Landslide scars are also observed at the Apennine mountains site (Salciarini *et al.,* 2006). Salciarini et al. (2006) studied slopes that ranged in overall steepness from 17.3º to 43.7º. This range cited suggests a similar critical slope angle of 40 – 45º, particularly since their data suggest a decrease in soil thickness of a factor 10 already for slope angle of 25 – 30º. These values are not greatly different from one another, meaning that the original value of 40º for the Olympic Mountains could perhaps be reasonably applied more generally, except in the SGM, where a more suitable estimate can be made. In fact, whenever no other viable options were available, we used all original erosion parameter values from the Olympic Mountains (Montgomery & Brandon, 2002).

In view of the rather extensive data and accompanying data descriptions, it was possible to generate reasonable values of all three erosion parameters for the San Gabriel Mountain (SGM; Table S1) sites investigated by Heimsath et al. (2012). Individual values for the SPR function are given at a wide range of slope angles, which can either be substituted directly into Eq. (9), or used to estimate values of the parameters for Eq. (13). At the SGM site, it is therefore possible to address the validity of both main inputs, Eq. (9) (or Eq. (6)) and Eq. (13), to Eq. (14) separately, since it is possible to find reasonable values for I and x_0 as well, similarly to Yu et al. (2017).

3.2. Sites Used for Comparison with Landslide Recovery, Eq. (1) or Eq. (7)

We start with the simplest case, initial soil development following a landslide. Altogether three sites for comparison with theory were found. These were located in New Zealand, Japan, and Switzerland. Only for the New Zealand and Switzerland sites could detailed information for extracting parameter values be found. The data for Shimokawa's (1984) site (with granitic substrate) was republished by Iida (1999) with ages determined by dendrochronology.

Taranaki Peninsula, North Island New Zealand

The Taranaki Peninsula extends southwestward from the city of Stratford on the southwestern coast of New Zealand. The Taranaki hill country 30 km to the east of Stratford is the site of the Trustrum & de Rose (1988) landslide recovery study. The yearly mean precipitation of the Taranaki study site is 1873mm (Trustrum & de Rose, 1988). The substrate is given as a silty sandstone (Trustrum & de Rose, 1988). The Taranaki Basin, which contains the only proven hydrocarbon reserves of New Zealand, extends from the hill country along the Peninsula to offshore. Its economic relevance has led to careful characterization. A study of the evolution of porosity in the Taranaki province was conducted by Armstrong et al. (1998) in order to deduce the exhumation magnitudes and erosion rates of this region. The study was conducted on

602 and near the Taranaki Peninsula which is located between 39º S and 39.5º S and at
603 about 174º E. The map of the authors extends to nearly 175º E and from 38º S to 41º
604 S. Armstrong et al. (1998) agree that the overlying rocks are a silty sandstone. The
605 porosity values of these sandstones trend from 50% offshore (173º E) to between
606 15% and 20% on the eastern margin near 175º E (Armstrong et al. 1998, Figure 6).
607 This information was used by Armstrong et al. (1998) to infer exhumation magnitudes
608 and corresponding denudation rates of 400 m Myr^{-1} at the eastern margin, and even
609 900m Myr^{-1} in the northeast. The southernmost onshore regions have a denudation
610 rate of 100-200m Myr^{-1}. A second reference, McBeath (1977), states on page 124 (in
611 reference to the Taranaki Basin sandstones), “The average porosity of gas-bearing
612 sands penetrated by the wells is 18.8%.” McBeath also noted that early 19^{th} Century
613 European settlers discovered oil seeping from the surface in this region. McBeath
614 (1977) also presents a table giving 15% as the average porosity of the
615 petroleum-bearing rocks. We used the value 18.8%.
616 A median particle diameter for a silt is 15µm, while for a sand it is approximately
617 115µm (Skaggs *et al.,* 2001). We take an arithmetic mean = 65 µm of 15µm and
618 115µm, since a silty sand should be closer to a sand than a silt. A similar result of
619 62µm is obtained using a geometric mean of 70% sand and 30% silt, for example.
620 The fraction of precipitation infiltrating was again assumed to be 23% (Lvovich, 1973).
621 After clearing of forest by European settlers, beginning in 1840, landslides occurred
622 rather frequently in the Taranaki hill country (Trustrum & de Rose, 1988). The
623 historical occurrence of many of these landslides allowed their dating with uncertainty
624 less than 1 year. The authors state, “Soil depths in landslide debris accumulation
625 zones are generally greater than 1.5m compared with an average depth of 0.7m on
626 hillslopes.” “Mean soil depths in the 30-40cm range have been observed on landslide
627 scars which appear to have slipped prior to forest clearance.” “Consequently, soils are
628 thinnest on ridges and spurs and thickest in swales and in footslopes, where soil
629 depths up to 3m have been observed.” The authors state, “Repeated landsliding on

630 previously failed surfaces has not been observed." "This suggests that new 'pasture'
631 soils have not yet reached a 'steady-state' depth, even after 80 years."
632
633 *Rossberg, Switzerland*
634 The Rossberg site is located in the northern part of the European Alps. The
635 geology of the Rossberg area is characterized by subalpine molasse. The alluvial
636 deposits are part of the Lower Freshwater Molasse (Lower Freshwater Molasse) of
637 the Oligocene. Due to its regular, geological structure with oblique, southward-dipping
638 layers, the southern side of the Rossberg mountain has been susceptible to
639 landslides. Historic and pre-historic landslides are known and were dated (for an
640 overview, see Egli & Fitze, 2001; Keller, 2017). The erosion data for the Rossberg site
641 (Table S2) were accessed from BAFU (2015) and soil characteristics from Meili
642 (1982) and BLW (2012). Programming and calculations were done using the software
643 R (R 3.3.2.). In order to facilitate reproducibility, the R code is made available under
644 https://github.com/curdon/soilDepth (Egli et al., 2018).
645
646 **3.3. San Gabriel Mountains (SGM) Parameters**
647
648 *Erosion-rate Parameters*
649 Instead of using purely statistical means to create the MB parameters for the
650 SGM, we have tried to take all the observations of the authors into account. The
651 contribution from a background erosion to soil production is suggested to be limited to
652 170m Myr^{-1} or less for slopes of less than about 30°, (from page 212) "Samples
653 collected across this more slowly eroding, convex-up part of the landscape define a
654 robust soil-production function, with SP_{max} equaling 170 ± 10m Myr^{-1}" while landsliding
655 contributes up to an additional 200m Myr^{-1} at steeper slopes, for a total erosion of
656 about 370m Myr^{-1}. "As morphology shifts from convex-up to planar, slope gradients
657 increase and we observed the soil mantle transition from being ubiquitous to

becoming increasingly patchy. We focused sampling of steep (average slope >30°) hillslopes on smooth, locally divergent ridges away from any landslide scars, thus ensuring that our ^{10}Be concentrations represent SPRs. Importantly, we observed that soil patches on threshold slopes, although typically thin (< 20cm) and coarse grained, are clearly produced locally and are not colluvial accumulations. SPRs from saprolite under these thin to non-existent soils are among the highest such rates ever reported, and exceed SP_{max} predicted from the low-relief soil pits by up to a factor of four, with a predicted maximum rate of 370 ± 40m Myr^{-1}." Heimsath et al. (2012) reported also a steepest observed slope of 45º that contained soil, meaning that the threshold slope angle is likely larger than 40º.

Other SGM Parameters

Sanford and Selnick (2012) give a precipitation range for the SGM of 51-75 cm. The middle of this range is 63 cm. The fraction corresponding to infiltration is, according to Lvovitch (1973), 23%, yielding 14.5cm yr^{-1}. Division by a typical porosity of 0.4 generates 36cm yr^{-1}. Soils in SGM, at least on hillslopes, are mainly loams (Rulli & Rosso, 2005), with median particle size ranging from 20 to 40μm (Skaggs *et al.,* 2001). Thus, we take 30μm as a typical particle size (Yu *et al.,* 2017). As noted, the range of reasonable values for each of the parameters is roughly a factor 2, though, e.g., adding variability in soil texture would increase this uncertainty.

3.4. Parameters for Testing Eq. (14): General Comments

Since at other sites, it was not possible to test Eq. (13) directly, we could test it only indirectly through by predicting the soil depth with Eq. (14). The near equivalence of Eq. (6) and a mean soil depth from Eq. (9) means that we can use Eq. (14) for

685 comparison with results from arbitrary landscapes, though with uncertainty in the
686 validity of the parameterization of the erosion rate.
687 In the comparison of the predictions of Eq. (14) with the slope angle,
688 complications from uncertainty in particle size and infiltration rate are reduced in a
689 relative sense. Consider that Eq. (14) is a power-law prediction of soil depth, inviting
690 logarithmic comparisons. On a bilogarithmic plot of soil depth against slope angle, the
691 only quantity which varies strongly is D, (though I can vary with a changing vertical
692 distance to bedrock, affected by local slope) and the net effect of changes in the two
693 constants, I and d_{50}, is essentially to raise or lower the curve by a constant value.
694 Rather than generating a new prediction for the combination of numerical factors
695 appropriate to each site, as long as the fundamental parameters from the erosion
696 model can be held constant, we can move each data set vertically, using the ratio of
697 its estimated combined numerical coefficient to a that of a known site. For the known
698 site, we choose the SGM. For the SGM, at least, we have prior estimations (Yu &
699 Hunt, 2017b) of I and d_{50}. At new sites we use this numerical combination as an
700 *adjustable* parameter, in order to see if the slope dependence, at least, of the soil
701 depth is properly accounted for. Then the optimal value of this parameter is compared
702 with our best estimate of what available information regarding I and d_{50} would imply.
703 If specific evidence for a different value of the critical slope could be found, we
704 took that qualitatively into account. Independent evidence for a background value of
705 the erosion rate and K were not generally available. The vertical shift in experimental
706 data is accomplished by rescaling particle diameters and infiltration rates to their
707 values in the SGM. d_{50} 10 times as great, i.e., 300μm, according to Eq. (14), generate
708 soils 10 times as deep; thus at a site where the measured particle d_{50} = 300μm, we
709 should account for that effect by dividing the experimental soil depths by 10. Effects of
710 variability in I are treated analogously. Since estimates of the worldwide variability of
711 mean deep infiltration rates range from 11% to 35% of annual precipitation,
712 (Schlesinger & Jasechko, 2014; Lvovich, 1973; Peel *et al.,* 2010), as in Yu et al.

(2017), we take the mean percentage (23%) of *P* to estimate *I* for each site. Such an estimation will introduce scatter, even if the estimated global mean is correct, since the mean value is not every value. Then, the ratio of the *I* value at each other site to the infiltration rate (0.36m yr^{-1}) in SGM is raised to the 1.15 power (as in Eq. (14)) to generate a second factor to relate the steady-state soil depth at the given site to the value in the SGM. We then normalize the soil depth based on the combined effect caused by the difference in both the particle size and infiltration rate, and the values are listed in Table 1.

3.5 Sites Used for Comparison with Soil Depth as Function of Slope, Eq. (14)

Appenine Mountains

For the Apennine Mountains, central Italy (Salciarini *et al.,* 2006), soils are mainly talus and are much coarser than SGM. We estimate the particle size based on the hydraulic conductivity (10^{-5} to 10^{-2} ms^{-1}) at the site (Salciarini *et al.,* 2006) and the authors' description of the soils as talus, an especially coarse material. From information provided by Aqtesolv, USGS and USDA, (accessed in Sep. 2017), comparable hydraulic conductivities are found within the category of coarse sand, which has particle size range from 600μm to 2000μm. The geometric mean of 1095μm is taken as the typical particle size.

Sterling

Soils at Sterling are mainly fine loamy and fine silty sand with percentage of sand ranging from 42% to 54% (Moore *et al.,* 1993), similar to the loamy texture in SGM, thus we applied the same particle sizes there as for SGM. When depth values are unavailable at slope close to zero, the deepest soil depths obtained (mostly in the valleys) in the field for each site are used as estimations of soil depths at zero slope.

These values may be affected by landslide deposits, but they are the only possible values to choose for normalization to zero slope.

Plastic Lake

Soil texture at Plastic Lake is not mentioned by the authors. We simply kept it as 30μm, the typical particle size of soil, which is calculated from the geometric mean of individual arithmetic means of the three principal soil particle classes, clay, silt, and sand. It is also known that silt is the middle particle size (geometric mean) class in soil classification schemes that has a mean value of 32μm, thus a 30μm of typical particle size would be a reasonable choice in the absence of any information regarding soil texture at Plastic Lake.

Norton & Smith

These data were simply digitized from a curve republished by Jenney (1941). Note that there was a slight upturn in the curve at the largest slope angles, which we attribute to a graphing error of the times.

4. Results and Discussion

For clarity, we first discuss model representations of the combined effects of gradual and threshold denudation processes before we address actual comparison with field measurements.

4.1. Relative Effects of Gradual and Threshold Denudation Processes

We now assess the relative contributions of gradual and catastrophic contributions to soil evolution at a point within the percolation framework. Specifically, we compare the value of t_l with the value of t_{ss}, a time to reach steady-state. Use of a

power-law decay in soil production rate does not permit the usual rigorous definition of a time scale consistent with an exponential decay, but a minimum time to reach steady-state can be found by setting the erosion-free soil depth at t_{ss} equal to the depth in steady-state. Thus we apply,

$$x = x_0 \left(\frac{t_{ss}}{t_0}\right)^{\frac{1}{D_b}} = x_0 \left(\frac{x_0/t_0}{DD_b}\right)^{\frac{1}{D_b - 1}} \qquad \text{Eq. (15)}$$

The solution of Eq. (15) can be represented in multiple ways. Two are given in Eq. (16).

$$t_{ss} = \frac{x_0}{DD_b} \left(\frac{I}{\emptyset DD_b}\right)^{\frac{1}{D_b - 1}} = \frac{x_{ss}}{DD_b} \qquad \text{Eq. (16)}$$

Here x_{ss} is the steady-state soil depth as obtained from (Eq. (6)). In the second form, t_{ss} is identifiable as proportional to the time it would take to remove the steady-state soil depth, x_{ss}, by a constant denudation rate, D, in the absence of soil production.

We can now consider the extreme cases of landslide-dominated and gradual erosion-dominated landscapes by comparing the two times, t_{ss} and t_l. Using Eq. (16), and the definition of t_l, one can see that the ratio of t_{ss}/t_l is a ratio of rates of erosion by landsliding and gradual processes. When $t_{ss} >> t_l$, landslide erosion rates are much larger than gradual contributions, and landslides occur long before soil development approaches the steady-state value generated by the gradual erosion processes. In this case, we can use Eq. (1) for soil depth in between landslides. Since this condition leads to a well-defined invertible relationship of $x_l(t_l)$, we can relate typical landslide occurrence intervals to a unique soil depth, implying that we can generate a prediction for a soil depth at which a given slope becomes unstable.

In the opposite case, when $t_l >> t_{ss}$, however, $x_l = x_{ss}$, since steady-state is virtually always reached before a landslide can occur. Further, since x_{ss} is independent of time, it is impossible to generate a unique time-depth relationship. The comparatively

796 rare process of landsliding always occurs at the same depth in a given location
797 (unless, e.g., climate changes), but at times which are completely unpredictable from
798 depth measurements, making landsliding effectively a purely random process to
799 which our analysis lends no predictive capability. Moreover, due to the spatially
800 variable infiltration rate alone, soil depths will also be spatially variable, even at the
801 same slope angle, but this variability still does not permit our approach to develop an
802 associated distinction in how close the respective slopes are to failure. Since the
803 importance of landsliding increases more rapidly with increasing slope angle than do
804 gradual processes, both cases $t_l >> t_{ss}$ and $t_{ss} >> t_l$ may develop in the same
805 geographic region, possibly even on the same hillslope. But, if a total denudation rate
806 can be identified that is valid across the range of slope angles found in a given region,
807 this relationship can be inserted into Eq. (6) to generate a prediction of soil depth, x,
808 whether this represents a steady-state value or an average value.
809 In the third case, when $t_l = t_{ss}$, there is some possibility for estimating slope
810 stability, but it is significantly degraded by the reduced sensitivity of depth to time.
811 Figure 1 shows a schematic diagram generated from our model with these three
812 different scenarios. The parameters we used to generate the curves are: I = 0.5m/yr,
813 x_0 = 100μm, and ϕ = 0.4. In the first case, we show what would result for a gradual
814 erosion rate of 100m Myr^{-1}, and no landsliding. For the second, we demonstrate the
815 appearance of the soil development including an erosion rate by landsliding of 100m
816 Myr^{-1} and zero gradual erosion. For the third we use 100m Myr^{-1} for both gradual and
817 landsliding processes, producing an approximate equality of t_{ss} and t_l.
818 What is illustrated, in the case of pure landsliding, is the power-law increase (with
819 power 0.53) of soil depth in time between landslides, then an abrupt loss of the entire
820 soil column at each landslide. This choice represents a further idealization. It is not
821 necessarily true that every landslide removes the entire soil column, particularly not at
822 every point. In the final case, Eq. (7) must be used to generate soil deepening
823 following landslides. For this choice of parameters, the soil depth is typically

approaching a steady-state value when the landslide occurs, but the variability in landslide recurrence intervals means that steady-state is sometimes reached and sometimes not at all.

If the present treatment of landsliding turns out to be of importance, the variability of t and x as given in Eq. (7) will constrain the particulars of any statistical approach applied to predict landsliding, since Eq. (7) is not a linear relationship.

4.2. Time-dependent Post-landslide Soil Recovery, Eq. (1) or Eq. (7)

Taranaki Peninsula, New Zealand

Of the three sites, consider first the Taranaki hill country site in New Zealand (Trustrum & de Rose, 1988). Figure 2a shows that insertion into Eq. (1) of the parameters given in the literature for porosity (18.8%), precipitation (1.873m/yr), and particle diameter (65 μm) leads to good agreement with field results using Eq. (1). The only parameter used which was not site-specific but a global mean, was the fraction of precipitation that infiltrates (between 11% and 35%, Lvovitch, 1973); these values bound the data reasonably well, although $I = 0.11\ P$ appears to be too low.

We can use Eq. (5) to calculate a steady-state depth for each of the denudation rates given by Armstrong et al. (1998). For 400m Myr^{-1}, the result is 0.66m, which compares well with the stated average hillslope depth of 0.7m. The smallest onshore denudation rates given by Armstrong et al. (1998) are 200m Myr^{-1} to 100m Myr^{-1}, which generate depths of 1.47m and 3.27m, respectively. These values compare well with the two values given by Trustrum & de Rose (1988) for “accumulation regions,” 1.5m, and for footslopes and swales (3m). Interestingly, the predicted soil depth for the 900m Myr^{-1} denudation rate is 0.26m, which is somewhat smaller than the 30-40cm of soil overlying pre-settlement landslide scars, but nevertheless suggests a possible inference that the variation in denudation rates is accommodated by the prevalence or rarity of landsliding. Note that regression of the four predicted and

852 observed steady-state soil depths, if the interpretations are legitimate, yields a slope
853 of 1.06 and an R^2 value of 0.992. Extrapolating Eq. (1) with the given parameters to a
854 depth of 35cm yields a time of 312 years, while use of Eq. (10) to generate a
855 steady-state time yields 389 years for the denudation rate of 900m Myr^{-1}. Thus, our
856 estimates of landslide recurrence intervals generate results between 2 and 2.5 times
857 the period since European settlement, in general accord with the conclusions of
858 Trustrum & de Rose (1988), that this time exceeds 80 years, and probably the time
859 since settlement.
860
861 *Japan*
862 The second site was in Japan (Shimokawa, 1984), for which no information to
863 suggest plausible values for I or d_{50} could be accessed. If the first data point in each of
864 the first two data sets is omitted, each conforms closely to Eq. (1), as seen in Figure
865 2b. The first data point from Shimokawa (1984) lies well above the trend, with the first
866 point of Trustrum & de Rose (1988), equally below. The resulting powers, 0.54 and
867 0.55 (predicted value 0.53), and relatively high R^2 values of 0.89 and 0.97, suggest
868 that, at both the Japan site and the New Zealand site, the time dependence of Eq. (1)
869 is confirmed.
870
871 *Rossberg, Switzerland*
872 The third site is Rossberg (Swiss Alps). Using Eq. (7), the predicted soil depths
873 match well with observed soil depths (Figure 3). The model slightly underestimates
874 soil depth for surface ages < 1000 years and probably slightly overestimates the soil
875 depth for older soils. The modelled trend rather displays a logarithmic function than a
876 power-law, although R^2 (based on the regression curve of plotted values and trend)
877 using a power-law is higher. However, Eq. (7) does predict power-law behavior only at
878 times short enough that it can be approximated by Eq. (1).
879

880 **4.3. Slope-Dependent Soil Depth, Eq. (14), with Specific Erosion Parameters**

881

882 *Parametrizing the MB Erosion Model Specifically for the SGM*

883

884 We apply the properties of the measured SPR for the erosion rates in order to
885 adapt the Montgomery & Brandon (2002) relationship to the SGM. We found E_0 = 40m
886 Myr^{-1}, S_c = 50º (not quite the Heimsath et al. (2012) value of 45º), and K = 2.3m Myr^{-1}.
887 These parameter values are for slopes expressed in degrees. We show the
888 comparison between predicted and observed SPRs in Figure 4. Note that the
889 modeled SPR reaches 170m Myr^{-1} at about 32.5º (close to the suggested cut-off of
890 30º) and 370m Myr^{-1} at 42º, in general accord with the authors' discussion and
891 assumed S_c of 45º. The value of about 600m Myr^{-1} at 45º is in accord with the only
892 data point (594m Myr^{-1} at 45º) for slopes greater than 40º.

893

894 *Results for Exponential and Percolation Soil Depth Predictions for the SGM*

895

896 We show results for the exponential formulation of the soil production function
897 first, and then the power-law formulation. In order to evaluate Eq. (3) for the Heimsath
898 et al. (2012) soil depth, it is necessary to select values of x_s and R_0. In Heimsath et al.
899 (2012) two different values for both R_0 (170m Myr^{-1} and 370m Myr^{-1}) and x_s are given
900 for the two different slopes, though the two x_s values are similar at about 30cm. Here,
901 no comparable distinction is made for the two slope ranges. Restricting to the single
902 value of R_{max} = 506m Myr^{-1}, and choosing x_s = 11.3cm, leads to the best fit, with a
903 slope of essentially 1 and an intercept of zero. The value of R^2 is unaffected by the
904 choice of parameters. This value of 506m Myr^{-1} is larger than all the experimentally
905 determined values except one (594m Myr^{-1}), which leads to the prediction of a
906 negative soil depth in that case. However, even the fit parameter 506m Myr^{-1} is larger
907 than the largest value characteristic of the highest slopes (370m Myr^{-1}) reported by

908 Heimsath et al. (2012). The result of the comparison is shown in Fig. 5a. Note that use
909 of a single SPR function requires a larger value of both the maximum SPR and a more
910 rapid decrease in SPR with depth than are reported in Heimsath et al. (2012), but the
911 discrepancies are not large.

912 Use of the percolation prediction leads to the comparison in Fig. 5b. Although
913 there are no adjustable parameters, the prediction is, on the average, off by only
914 about 14%, while the R^2 value is noticeably greater than obtained for the exponential
915 phenomenology, 0.59 instead of 0.39. Here, we have for three sites replaced the
916 extremely low measured SPR values by values expected from the MB formulation.
917 We can give three reasons for this; first, the measured SPR values give soil depths
918 that are much too large; secondly, the measured SPR values are much smaller than
919 any others with similar slopes, and third, the regression for the SPR as a function of
920 soil depth given in Heimsath et al. (2012) is not consistent with these three sites
921 either. In the first argument, the three SPR values correspond to erosion rates of 12m
922 Myr^{-1}, 21m/Myr^{-1} and 10m/Myr^{-1} for slopes with angles 17º, 0º, and 5º, respectively.
923 The MB phenomenological result with best fit parameters for the SGM yields erosion
924 rates of 84m/Myr^{-1}, 40m Myr^{-1}, and 52m Myr^{-1}, however, for these three slope angles.
925 If the values obtained from the fit of the MB erosion rate to the data are used for the
926 erosion rates at these three sites, then adding these three sites back to the analyzed
927 data is completely consistent with the remaining data points. (The addition of these
928 three points produces only a small change in the R^2 value, from 0.583 to 0.586).
929 Moreover, the Heimsath regression for slopes less than 30º, R = 170m Myr^{-1} exp
930 (-0.031x) yields 32m Myr^{-1} for the deepest soils measured (x = 54cm). This value of
931 32m Myr^{-1} is also only 20% smaller than the background denudation rate of 40m
932 Myr^{-1}, which we used to generate the best-fit parameters for the MB phenomenology,
933 but triple the smallest SPR values measured.

934 The comparisons of theory with experiment may also be put on a single graph
935 (Fig. 6) showing results from both the exponential depth dependence of the SPR and

936 the percolation theoretical result. The most obvious distinction is the negative
937 curvature of the predicted results from the exponential phenomenology. An alternative
938 representation is to plot both predicted and observed depths for each site as functions
939 of slope angle (Fig. 7). Although the soil depth is represented as a function of slope
940 angle, it is calculated here point-by-point from the observed, rather than modeled, soil
941 production function. The reason that the R^2 value for the percolation treatment (0.59)
942 is higher than that for the exponential model (0.39) is now visible. The advantage is
943 associated with the wider range of predicted soil depths at any given slope using the
944 percolation model on account of its greater sensitivity to the SPR. Thus, the
945 exponential model predictions tend to lie more nearly in the center of the envelope of
946 measured soil depths at a given slope angle.
947 It is interesting to use the Montgomery and Brandon erosion rate phenomenology,
948 which was tested on the actual SPR data from the SGM, to generate a steady-state
949 soil depth across the SGM sites by both percolation and exponential representations,
950 as well as the percolation result for maximum soil depth attained between landslides.
951 The result is shown in Fig. (8). For most of the range of slope angles, the distinction
952 between the steady-state percolation and exponential phenomenologies is small, but
953 it should be noted that the percolation parameters were determined from other
954 measurements, rather than from an optimal agreement with experiment. If the
955 maximum percolation prediction using the MB slope erosion-rate function and the full
956 time between landslides is indeed reliable, one could infer that the 8 (of a total 55)
957 sites above this curve are susceptible to landslides, except that the authors (Heimsath
958 et al. 2012) noted specifically that they tried to avoid this eventuality by picking sites
959 with rounded topography near ridge crests. Nevertheless, Figure 9. shows the close
960 proximity of two such sites to landslide scars.
961 Finally, it should be noted that the maximum soil depth from the stochastic
962 solution seems to provide an upper limit for soil depths only at slopes larger than
963 approximately 10-15º, roughly in accord with the authors' observation that such

964 landsliding is dominant only on slopes greater than 30º. At slope angles smaller than
965 10º, the upper bound for soil depths is more nearly consistent with the steady-state
966 percolation calculation, a factor 2 smaller.
967
968 **4.4. Slope-dependent Soil Depth, Eq. (14), Imported Erosion Parameters**
969
970 Figure 10 shows a comparison of the slope-dependent development of soils in
971 three studies of gradual soil erosion (Moore *et al.,* 1993; Buttle *et al.,* 2004; Norton &
972 Smith (1930) as digitized from Jenny, 1941), as well as one case, the Appenine
973 Mountians (AM) where soil erosion is predominantly by landsliding (Salciarini *et al.,*
974 2006). The identical function (Eq. 14) with the same erosion parameters as for the
975 Olympic Mountains was used to predict all soil depths. Note that the Norton and Smith
976 data were already considered in Yu et al. (2017a). However, in each of the four cases
977 the data were multiplied by a constant factor, representing distinctions in particle size
978 and infiltration rates, in order to generate closest agreement with Eq. (16). We
979 investigated the sensitivity of the comparison to the values of these constants and
980 found that they are accurate within about 5%. The resulting four “fit” prefactors are
981 given in Table 1. Four corresponding parameter values, as estimated from
982 comparison with the particle size and infiltration data of the SGM, are also given in
983 Table 1. Comparing the values pairwise suggests that our theoretically-based
984 estimates are generally within a factor 2 or less of the best-fit values.
985 What we infer from this comparison is: 1) the soil production model appears to be
986 in accord with these data as well, 2) the erosion model of Montgomery and Brandon
987 (2002) is probably applicable in a wide range of cases, since it is compatible with all
988 the data considered here, although two distinct sets of parameter values needed to be
989 employed, one for the SGM, and a second for the other 4 sites.
990
991 **5. Conclusions**

The soil formation model derived from percolation theory can be used to predict soil recovery after landslides. In its steady-state form, it can also be used to generate an expression for a mean soil depth as a function of slope by adopting an appropriate relationship between erosion rate and slope angle. Addressing the slope dependence of soil depths introduces additional possibilities to test the predictions, but also introduces additional uncertainties in input parameters. At steep slopes, where erosion of soil is mass wasting-dominated or susceptible to shallow landsliding, the steady-state predicted soil depth may be interpreted as a temporal and/or spatial mean soil depth. The predicted soil depth neglecting gradual erosion, but evaluated at landslide recurrence intervals, is a factor 2 larger than the steady-state soil depth prediction for the same total erosion rate. The mean soil depth in threshold landscapes is not greatly different from that where steady-state models are appropriate, as long as the total erosion rate is the same. Using a single published relationship for the erosion rate as a function of slope angle, it is possible to generate a quasi-universal prediction of mean soil depth as a function of slope angle. For both the case where gradual erosion processes dominate and when landsliding dominates erosion, the soil depths predicted thus are often in very close agreement with observed depths. It appears likely that the present formulation of soil depth as a function of erosion rate has the potential to explain slope angle dependences of soil depth as well, provided it is possible for any given geographic region to generate a reliable model of erosion rate as a function of slope angle. Even though Heimsath et al. (2012) explicitly avoided measuring soil production rates on landslide scars at steeper slopes, our predictions regarding stability mapped out rather accurately the maximum soil depth observed as a function of slope angle, while those sites with slightly greater depths were sometimes found adjacent to landslide scars. Thus, a method to generate a maximum stable soil depth as a function of slope angle may provide a means to distinguish soils susceptible to landsliding.

Acknowledgements

This research was supported by the Swiss National Science Foundation (SNSF) project grant no. IZSEZ0_180377 / 1.

All primary data and the modeling code are available in the supplementary material.

References

Aqtesolv, USGS and USDA websites (accessed in Sep. 2017):
http://www.aqtesolv.com/aquifer-tests/aquifer_properties.html
https://pubs.usgs.gov/wri/1995/4160/report.pdf
https://www.nrcs.usda.gov/wps/portal/nrcs/detail/soils/survey/office/ssr10/tr/?cid=nrcs144p2_074846

Ahnert, F. (1970). Functional relationship between denudation relief and uplift in large mid-latitude drainage basins. *American Journal of Science* ***268****:* 243–263. DOI: 10.2475/ajs.268.3.243

Anderson, R. S. & Anderson, S. P. (2010). *Geomorphology: the mechanics and chemistry of landscapes*. Cambridge University Press, New York.

Armstrong, P. A., Allis, R. G., Funnell, R. H., & Chapman, D. S. (1998). Late Neogene exhumation patterns in the Taranaki Basin (New Zealand): Evidence from offset porosity-depth trends, *Journal of Geophysical Research* ***103***: 30269-30282. DOI: 10.1029/98JB02843

BAFU (Bundesamt für Umwelt). (2015). *Hydrologischer Atlas der Schweiz*. Geographisches Institut der Universität Bern, Bern. http://hydrologischeratlas.ch/

Bierman, P. R., & Nichols, K. K. (2004). Rock to sediment-slope to sea with ^{10}Be rates of landscape change. *Annual Review of Earth and Planetary Sciences* **32**, 215–255. DOI: 10.1146/annurev.earth.32.101802.120539

Binnie, S. A., Phillips, W. M., & Summerfield, M. A. (2007). Tectonic uplift, threshold hillslopes, and denudation rates in a developing mountain range. *Geology* **35**, 743–746. DOI: 10.1130/G23641A.1

Blanco, H., & Lal, R. (2010), Principles of Soil Conservation and Management, Springer, Heidelberg.

BLW (Bundesamt für Landwirtschaft) (2012). *Digitale Bodeneignungskarte der Schweiz*. Bern.

1053 Braun, J., Mercier, J., Guillocheau, F., & Robin, C., (2016). A simple model for regolith
1054 formation by chemical weathering. *J. Geophys. Res. Earth Surface* **121**:
1055 2140-2171. DOI: 10.1002/2016JF003914
1056 Braun, J., Guillocheau, & Robin, C., (2017). Reply to Comment on “A simple model for
1057 regolith formation by chemical weathering,” by Braun et al. Contradictory
1058 concentrations and a tale of two velocities by Harman et al. *J. Geophys. Res. Earth*
1059 *Surface* **122**: 2037-2039. DOI: 10.1002/2017JF004271
1060 Burbank. D. W., Leland, J., Fielding, E., Anderson R. S., Brozovic, N., Reid, M. R., &
1061 Ducan, C. (1996). Bedrock incision, rock uplift and threshold hillslopes in the
1062 northwestern Himalayas. *Nature,* **379**, 505–510. DOI: 10.1038/379505a0
1063 Burke, B. C., Heimsath, A. M., & White, A. F. (2006). Coupling chemical weathering
1064 with soil production across soil-mantled landscapes. *Earth Surface Processes and*
1065 *Landform*s, **32**: 853-873. DOI: 10.1002/esp.1443
1066 Burke, B. C., Heimsath, A. M., Chappell, J., & Yoo, K. (2009). Weathering the
1067 escarpment: Chemical and physical rates and processes, southeastern Australia.
1068 *Earth Surface Processes and Landforms* **34**, 768-785. DOI: 10.1002/esp.1764
1069 Buttle, J. M., Dillon, P. J., & Eerkes, G. R. (2004). Hydrologic coupling of slopes,
1070 riparian zones and streams: an example from the Canadian Shield. *Journal of*
1071 *Hydrology* **287**, 161–177. DOI: 10.1016/j.jhydrol.2003.09.022
1072 Buttle, J. M., & House, D. A. (1997). Spatial variability of saturated hydraulic
1073 conductivity in shallow macroporous soils in a forested basin. *Journal of Hydrology*
1074 **203**, 127–142. DOI:10.1016/S0022-1694(97)00095-4
1075 Carson, M. A., & Petley, D. J. (1970). Existence of threshold hillslopes in denudation
1076 of landscape. *Institute of British Geographers Transactions* **49**, 71–95. DOI:
1077 10.2307/621642
1078 Claessens, L., Knapen, A., Kitutu, M. G., Poesen, J., & Deckers, J. A. (2007).
1079 Modelling landslide hazard, soil redistribution and sediment yield on the Ugandan

1080 footslopes of Mt. Elgon. *Geomorphology* **90**: 23-35. DOI:
1081 10.1016/j.geomorph.2007.01
1082 Darwin, C. (1881). The Formation of Vegetable Mould through the Action of Worms,
1083 with Observations on Their Habits; John Murray: London, UK.
1084 DiBiase, R. A., Whipple, K. X., Heimsath, A. M., & Ouimet, W. B. (2010). Landscape
1085 form and millennial erosion rate in the San Gabriel Mountains, CA. *Earth and*
1086 *Planetary Science Letters **289**:* 134–144. DOI: 10.1016/j.epsl.2009.10.036
1087 DiBiase, R. A., Heimsath, A. M., & Whipple, K. X. (2012). Hillslope response to
1088 tectonic forcing in threshold landscapes. *Earth Surface Processes and Landforms,*
1089 **289***:* 134–144. DOI: 10.1016/j.epsl.2009.10.036
1090 Dietrich, W. E., Reiss, R., Hsu, M.-L., & Montgomery, D. (1995). A process-based
1091 model for colluvial soil depth and shallow landsliding using digital elevation data,
1092 Hydrological Processes **9**: 383-4000. DOI: 10.1002/hyp.3360090311
1093 Dietrich, W. E., McKean, J., Bellugi, D. & Perron, T. (2007). The prediction of shallow
1094 landslide location and size using multidimensional landslide analysis in a digital
1095 terrain model in Chen, C. L. ; Major, J. J. Eds. Proceedings of the Fourth
1096 International on Debris-Flow Hazards Mitigation: Mechanics, Prediction and
1097 Assessment (DFHM-4) The Netherlands, Amsterdam: IOS Press 12 p.
1098 Dixon, J. L., Heimsath, A. M., Kaste, J., & Amundson, R. (2009a). Climate-driven
1099 processes of hillslope weathering. *Geology,* **37**: 975-978. DOI: 10.1130/G30045A.1
1100 Dixon, J. L., Heimsath, A. M., & Amundson, R. (2009b). The critical role of climate and
1101 saprolite weathering in landscape evolution. *Earth Surface Processes and*
1102 *Landforms,* **34**: 1507-1521. DOI: 10.1002/esp.1836
1103 Dokuchaev, V. V. (1948). *Russian Chernozem* – Selected works of V. V. Dokuchaev,
1104 Volume I. Moskva, 1948. Translated from the Russian by Israel Program for
1105 Scientific Translations, Jerusalem, 1967.

1106 Dunne, T., W. Zhang, & Aubry, B. F. (1991). Effects of rainfall, vegetation, and
1107 microtopography on infiltration and runoff. *Water Resources Research* **27**:
1108 2271-2285. DOI: 10.1029/91WR01585
1109 Egli, M., & Fitze, P. (2001). Quantitative aspects of carbonate leaching of soils with
1110 differing ages and climates. *Catena,* **46**: 35-62. DOI:
1111 10.1016/S0341-8162(01)00154-0.
1112 Egli, M., Dahms, D., & Norton, K. (2014). Soil formation rates on silicate parent
1113 material in alpine environments: Different approaches–different results?
1114 *Geoderma,* **213**: 320–333. DOI: 10.1016/j.geoderma.2013.08.016
1115 Egli, M., Hunt, A., Dahms, D., Raab, G., Derungs, C., Raimondi, S., & Fang, Y.
1116 (2018). Prediction of soil formation as a function of age using the percolation theory
1117 approach. *Frontiers in Environmental Science,* **6**: 108, doi:
1118 10.3389/fenvs.2018.00108.
1119 Eppes, M. C., & Keanini, R. (2017). Mechanical weathering and rock erosion by
1120 climate-dependent subcritical cracking. *Reviews of Geophysics* **55**: 470-508. DOI:
1121 10.1002/2017RG000557
1122 Gilbert, G. K. (1877). *Report on the geology of Henry Mountains*. US Geological and
1123 Geographical Survey of the Rock Mountain Region. Government of Printing Office,
1124 Washington DC.
1125 Harman, C. J., Cosans, C. L., & Putnam, S. M. (2017). Comment on “A simple model
1126 for regolith formation by chemical weathering” by Braun et al.: Contradictory
1127 concentrations and a tale of two velocities, Journal of Geophys. Res. Earth Surface
1128 **121(11)**: 2140-2171. DOI: 10.1002/2016JF003914
1129 Hartmann, J., Moosdorf, N., Lauerwald, R., Hinderer, M., & West, J. A. (2014). Global
1130 chemical weathering and associated P-release: The role of lithology, temperature
1131 and soil properties. Chemical Geology **363**: 145-163. DOI:
1132 10.1016/j.chemgeo.2013.10.025

1133 Heimsath, A. M., Dietrich, W. E., Nishiizumi, K., & Finkel, R. C. (1997). The soil
1134 production function and landscape equilibrium. *Nature* **388**: 358–361. DOI:
1135 10.1038/41056
1136 Heimsath, A. M., Dietrich, W. E., Nishiizumi, K., & Finkel, R. C. (1999). Cosmogenic
1137 nuclides, topography, and the spatial variation of soil depth. *Geomorphology* **27**:
1138 151–172. DOI: 10.1016/S0169-555X(98)00095-6
1139 Heimsath, A.M., Furbish, D.J., & Dietrich, W.E. (2005). The illusion of diffusion: Field
1140 evidence for depth-dependent sediment transport. *Geology* **33***,* 949–952, DOI:
1141 10.1130/G21868.1.
1142 Heimsath, A. M., DiBiase, R. A., & Whipple, K.X. (2012). Soil production limits and the
1143 transition to bedrock-dominated landscapes. *Nature Geoscience* **5**: 210-214. DOI:
1144 10.1038/NGEO1380
1145 Hillel, D. 2005. Soil: Crucible of life. *J. Nat. Resour. Life Sci. Educ*.**34**, 60–61.
1146 Hunt, A. G., & Skinner, T. E. (2008). Longitudinal dispersion of solutes in porous
1147 media solely by advection. *Philosophical Magazine* **88**: 2921–2944. DOI:
1148 10.1080/14786430802395137
1149 Hunt, A. G., & Sahimi, M. (2017). Flow, transport, and reaction in porous media:
1150 Percolation scaling, critical path analysis and effective-medium approximation.
1151 *Reviews of Geophysics* **55**: 993-1078. DOI: 10.1002/2017RG000558
1152 Hunt, A. G., & Ghanbarian, B. (2016). Percolation theory for solute transport in porous
1153 media: Geochemistry, geomorphology, and carbon cycling. *Water Resource*
1154 *Research* **52**: 7444–7459. DOI: 10.1002/2016WR019289
1155 Huntly, N., & Inouye, R. (1988). Pocket gophers in ecosystems: Patterns and
1156 mechanisms, BioScience 38: 786-793 DOI: 10.2307/1310788
1157 Hurst, M. D., Mudd, S. M., Walcott, R., Mikael, A., & Yoo, K. (2012). Using hilltop
1158 curvature to derive the spatial distribution of erosion rates. *Journal of Geophysical*
1159 *Research* **117**: F02017. DOI: 10.1029/2011JF002057

1160 Iida, T. (1999). A stochastic hydro-geomorphological model for shallow landsliding
1161 due to rainstorm. *Catena* **34**: 293–313. DOI: 10.1016/S0341-8162(98)00093-9
1162 Jenny, H. (1941). *Factors of soil formation*: *a system of quantitative pedology;* Dover:
1163 New York.
1164 Jones, F. O. (1973). Landslides of Rio de Janeiro and the Serra das Araras
1165 escarpment, Brazil. *U.S. Geological Survey Professional Paper* **697**: 42. DOI:
1166 10.3133/pp697
1167 Johnson, D. L., and Schaetzl, R. J. (2015). Differing views of soil and pedogenesis by
1168 two masters: Darwin and Dokuchaev, *Geoderma* **237-238**: 176-189. DOI:
1169 10.1016/j.geoderma.2014.08.020
1170 Keller, B. (2017). Massive rock slope failure in Central Switzerland: history,
1171 geologic-geomorphological predisposition, types and triggers, and resulting risks.
1172 *Landslides* **14**: 1633-1653. DOI: 10.1007/s1034
1173 Kump, L. R., Brantley, S. L., & Arthur, M. A. (2000). Chemical weathering,
1174 atmospheric CO2 and climate, Ann. Rev. Earth Planet Sci. **28**: 611-67. DOI:
1175 10.1146/annurev.earth.28.1.611
1176 Larsen, I. J., Almond, P. C., Eger, A., Stone, J. O., Montgomery, D. R., & Malcolm, B.
1177 (2014). Rapid soil production and weathering in the Southern Alps, New Zealand.
1178 *Science* **343**: 637–640. DOI: 10.1126/science.1244908
1179 Lvovitch, M. I. (1973). The global water balance: U.S. National Committee for the
1180 International Hydrological Decade. *U.S. National Committee for the International*
1181 *Hydrological Decade Bulletin* **23**: 28–42. DOI: 10.1029/EO054i001p00028
1182 Maher, K. (2010). The dependence of chemical weathering rates on fluid residence
1183 time, *Earth Plan. Sci. Lett.* **294**: 101–110. DOI: 10.1016/j.epsl.2010.03.010
1184 McBeath, D. M. (1977). Gas-condensate fields of the Taranaki Basin. *New Zealand*
1185 *Journal of Geology and Geophysics* **20**: 99-127. DOI:
1186 10.1080/00288306.1977.10431594

1187 Meili, R. B. (1982). *Untersuchungen zur Bodenentwicklung im Bergsturzgebiet des*
1188 *Rossbergs*. Unpubl. diploma thesis. Geograph. Institut Univ. Zürich.
1189 Montgomery, D.R. (2001). Slope distributions, threshold hillslopes, and steady-state
1190 topography. *American Journal of Science* **301**: 432–454. DOI:
1191 10.2475/ajs.301.4-5.432
1192 Montgomery, D. R., & Brandon, M. T. (2002). Topographic controls on erosion rates in
1193 tectonically active mountain ranges. *Earth and Planetary Science Letters* **201**: 481–
1194 489. DOI: 10.1016/S0012-821X(02)00725-2
1195 Montgomery, D. (2007a). Soil erosion and agricultural sustainability, Proceedings of
1196 the National Academy of Sciences **104**: 13268-13272. DOI:
1197 10.1073/pnas.0611508104
1198 Montgomery, D. (2007b). Dirt, The Erosion of Civilization, University of California
1199 Press, 295 pp. ISBN: 9780520248700
1200 Montgomery, D. R., & Brandon, M.T. (2002). Topographic controls on erosion rates in
1201 tectonically active mountain ranges. Earth and Planetary Science Letters 201: 481–
1202 489. DOI: 10.1016/S0012-821X(02)00725-2
1203 Moore, D., Gessler, P. E., Nielsen, G. A., & Peterson, G. A. (1993). Soil attribute
1204 prediction using terrain analysis. *Soil Science Society of American Journal* **57**:
1205 443–452. DOI:10.2136/sssaj1993.03615995005700020026x
1206 Norton, E. A., & Smith, R. S. (1930). The influence of topography on soil profile
1207 character *J. Amer. Soc. Of Agronomy* **22**: 251-262.
1208 Okimura, T. (1987). Investigation and countermeasure of surface failures. *Chisitsu to*
1209 *tyosa,* **33**: 22–28.
1210 Ouimet, W. B., Whipple, K. X, & Granger, D. E. (2009). Beyond threshold hillslope:
1211 channel adjustment to base-level fall in tectonically active mountain ranges.
1212 *Geology* **37**: 579–582. DOI: 10.1130/G30013A.1

1213 Owen, J. J., Amundson, R., Dietrich, W. E., Nishiizumi, K., Sutter, B., & Chong, G.
1214 (2010). The sensitivity of hillslope soil production to precipitation. *Earth Surface*
1215 *Processes and Landforms* **36**: 117-135. DOI: 10.1002/esp.2083
1216 Pawlik, L., Phillips, U. D., & Samonil, P. (2016) Roots, rock, and regolith:
1217 Biomechanical and biochemical by trees and its impact on hillslopes – A critical
1218 literature review. *Earth Science Reviews* **159**: 142-159. DOI:
1219 10.1016/j.earscirev.2016.06.002
1220 Pazzaglia, F. J., & Brandon M. T. (1996). Macrogeomorphic evolution of the
1221 post-Triassic Appalachian Mountains determined by deconvolution of the offshore
1222 basin sedimentary record. *Basin Research* **8**: 255-278. DOI:
1223 10.1046/j.1365-2117.1996.00274.x
1224 Peel, M. C., McMahon, T. A., & Finlayson, B. L. (2010). Vegetation impact on mean
1225 annual evapotranspiration at a global catchment scale. *Water Resource Research*
1226 **46**: W09508. DOI: 10.1029/2009WR008233
1227 Phillips, J. D. (2010). The convenient fiction of steady-state soil thickness. *Geoderma,*
1228 **156**: 389-398. DOI: 10.1016/j.geoderma.2010.03.008.
1229 RAC DSR Report. (2009). Anaconda evaporation ponds removal action
1230 characterization data summary report revision I.
1231 https://yosemite.epa.gov/r9/sfund/r9sfdocw.nsf/3dc283e6c5d6056f882574260074
1232 17a2/2fad55aa1c0a3f618825767200822686!OpenDocument
1233 Roering, J. J., Perron, J. T., & Kirchner, J. W. (2007). Functional relationships
1234 between denudation and hillslope form and relief. *Earth and Planetary Science*
1235 *Letters* **264**: 45–258. DOI: 10.1016/j.epsl.2007.09.035
1236 Roering, J.J. (2008). How well can hillslope evolution models “explain” topography?
1237 Simulating soil transport and production with high-resolution topographic data.
1238 *Geological Society of America Bulletin* **120**: 1248–162. DOI: 10.1130/B26283.1

1239 Rulli, M. C., Rosso, R. (2005). Modeling catchment erosion after wildfires in the San
1240 Gabriel Mountains in the southern California. *Geophysical Research Letters* **32**:
1241 L19401. DOI: 10.1029/2005GL023635.
1242 Sahimi, M. (1994). *Applications of Percolation Theory*. Taylor & Francis, London.
1243 Salciarini, D., Godt, J. W., Savage, W. Z., Conversini, P., Baum, R. L., & Michael, J. A.
1244 (2006). Modeling regional initiation of rainfall-induced shallow landslides in the
1245 eastern Umbria Region of central Italy. *Landslides* **2**: 181–194. DOI:
1246 10.1007/s10346-006-0037-0
1247 Sanford, W. E., & Selnick, D. L. (2013). Estimation of evapotranspiration across the
1248 conterminous United States using a regression with climate and land-cover data, *J.*
1249 *Am. Water Res. Assoc.* **49**: 217-230. DOI: 10.1111/jawr.12010
1250 Schlesinger, W. H., & Jasechko, S. (2014). Transpiration in the global water cycle.
1251 *Agricultural and Forest Meteorology* **189**: 115–117. DOI:
1252 10.1016/j.agrformet.2014.01.011
1253 Schmidt, K. M., & Montgomery, D. R. (1995). Limits to relief. *Science* **270**, 617–620.
1254 DOI: 10.1126/science.270.5236.617.
1255 Shimokawa, E. (1984). A natural recovery process of vegetation on landslide scars
1256 and landslide periodicity in forested drainage basins. In: O'Loughlin CL, Pierce AJ
1257 (eds) *Proceedings of the Symposium on effects of forest land use on erosion and*
1258 *slope stability* (pp. 99–107).
1259 Sheppard, A. P., Knackstedt, M. A., Pinczewski, W. V., & Sahimi, M. (1999). Invasion
1260 Percolation: New Algorithms and Universality Classes. *Journal of Physics A:*
1261 *Mathematical and General* ***32***: L521–L529 ISSN: 0305-4470
1262 Skaggs, T.H., Arya, L.M., Shouse, P.J., & Mohanty, B. (2011). Estimating particle-size
1263 distribution from limited soil texture data. *Soil Science Society of America Journal*
1264 **65**: 1038–1044. DOI: 10.2136/sssaj2001.6541038x
1265 St. Clair, J., Moon, S., Holbrook, W.S., Perron, J.T., Riebe, C.S., Martel, S.J., Carr, B.,
1266 Harman, C., & Singha, K. (2015). Geophysical imaging reveals topographic stress

1267 control of bedrock weathering. Science, 350(6260), 534-538. DOI:
1268 10.1126/science.aab2210
1269 Trustrum, N. A., & De Rose, R. C. (1988). Soil depth-age relationship of landslides on
1270 deforested hillslopes, Taranaki, New Zealand. *Geomorphology* **1**: 143–160. DOI:
1271 10.1016/0169-555X(88)90012-8
1272 Von Blanckenburg, F. (2005). The control mechanisms of erosion and weathering at
1273 basin scale from cosmogenic nuclides in river sediments. *Earth and Planetary*
1274 *Science Letters* **237**: 462-479. DOI: 10.1016/j.epsl.2005.11.017
1275 White A. F., & Brantley S. L. (2003). The effect of time on the weathering rates of
1276 silicate minerals. Why do weathering rates differ in the lab and in the field? *Chem.*
1277 *Geol.* **202**, 479-506. DOI: 10.1016/j.chemgeo.2003.03.001
1278 Yoo, K., Amundson, R., Heimsath, A. M., & Dietrich, W. E. (2005) Process-based
1279 model linking pocket gopher (Thomomys bottae activity to sediment transport and
1280 soil thickness, Geology 33: 917-920 doi: 10.1130/G21831.1
1281 Yu F., & Hunt, A. G. (2017a). An Examination of the Steady-State Assumption in Soil
1282 Development Models with Application to Landscape Evolution. *Earth Surface*
1283 *Processes and Landforms* **42**: 2599-2610. DOI: 10.1002/esp.4209
1284 Yu F., & Hunt, A. G. (2017b). Damköhler number input to transport-limited chemical
1285 weathering calculations. *ACS Earth and Space Chemistry* **1**: 30–38. DOI:
1286 10.1021/acsearthspacechem.6b00007
1287 Yu F., & Hunt, A. G. (2017c). Predicting of soil formation on the basis of
1288 transport-limited chemical weathering. *Geomorphology* **201**: 21–27. DOI:
1289 10.1016/j.geomorph.2017.10.027
1290 Yu, F., Faybishenko, B., Hunt, A. G., & Ghanbarian-Alavijeh, B. (2017). A simple
1291 model of the variability of soil depths. *Water* **9**: 460. DOI: 10.3390/w9070460

Figure captions

Figure 1. Schematic illustration of soil depths with and without disturbance of shallow landsliding as well as background erosion over time. Red curve includes 100m/Myr soil loss from gradual processes, but no landsliding, blue curve includes 100m/Myr soil loss from landsliding, but no soil loss from gradual processes, while the green curve includes 100m/Myr soil loss from each of the gradual and catastrophic processes. Time of blue curve is generated aperiodically at ages of 5000, 7000, 15000, 40000, and 60000 years. Time of green curve is generated at ages of 2000, 5000, 7000, 15000, 40000, 60000,70000, and 95000 years.

Figure 2. a) Estimated soil depth development in time at the Taranaki site in New Zealand (Trustrum and de Rose, 1988) compared with observed soil depths. Short dashed curve corresponds to $I = 0.11\ P$, long dashes to $I = 0.35\ P$, and the solid line to $I = 0.23\ P$. Other parameters are described in the text. b) Scaling of soil development with age of landslide scars. Data from Shimokawa (1984) is digitized from Iida (1999, Figure 11). First data point at 4 yrs, which is well above the trend line, was omitted. For data from Trustrum and De Rose (1988), first data point at 13yr, well below the trend line, is neglected. Multiple soil depths at 15 years are averaged to reduce scatter.

Figure 3. a) Post-landslide soil development at Rossberg, Switzerland as compared with theoretical predictions from Eq. (6). The predictions are made without use of adjustable parameters and include a significant background soil loss from gradual erosion processes, noted particularly at time scales exceeding about 5,000 years. b)

1319 Comparison between modeled and measured values. The 1:1 relationship is given by
1320 the dashed line.
1321
1322
1323 **Figure 4.** Fit of Montgomery-Brandon (MB) phenomenological relationship for erosion
1324 as a function of slope angle to data (Heimsath et al. 2012) for soil production rates as
1325 a function of slope angle for the SGM. Parameters are given in the text.
1326
1327
1328 **Figure 5.** a) Optimized fit for soil depths as a function of soil production rates using
1329 exponential phenomenology of Heimsath et al. (2012) and a single maximum soil
1330 production rate. Data for the SGM from Heimsath et al. (2012). b) For the same site
1331 and data, comparison of percolation predictions for soil depths using observed soil
1332 production rates.
1333
1334
1335 **Figure 6.** Comparison of exponential phenomenology with percolation prediction and
1336 data from the SGM. In this case, the parameters of the exponential phenomenology
1337 were chosen in order to generate similar predicted soil depths as obtained from
1338 percolation concepts, in order to emphasize the difference in curvature from the two
1339 models. The maximum SPR = 300m/Myr and x_0 = 25cm were applied, in each case
1340 within 20% of the values Heimsath et al. (2012) used for steeper slopes. Description
1341 of terms: Heimsath stoch.: stochastic means in this context that all erosion is due to
1342 landsliding; Eq. 12. Heimsath steady state: according to Eq. 3
1343 Percolation steady state: according to Eq. 16
1344
1345

Figure 7. a) Comparison of predicted and observed soil depths as a function of slope angle using the exponential phenomenology and the best fit parameters given in the text. b) Comparison of predicted and observed soil depths using percolation theory for chemical weathering and best estimates for input parameters as discussed in text.

Figure 8. Comparison of exponential fit and percolation prediction for soil depths as a function of slope angle. Description of terms: MB = Montgomery & Brandon (2002), Eq. 15. Percolation prediction: Eq. (6) with measured values of SPR for erosion rates. Percolation steady state: according to Eq. 16. Heimsath: Eq. (3) with MB (Eq. (15) substituted for the denudation rate, *D*. Percolation Stochastic: Eq. (9) with MB (Eq. 15)

Figure 9. Images of two sites (Heimsath et al., 2012) with actual soil depths exceeding predicted values from stochastic application of percolation theory to maximum stable soil depth in landslide prone areas.

Figure 10. Comparison of predicted soil depth and observed soil depth at 3 study sites exhibiting gradual erosion. PL = Plastic Lake (Buttle *et al.,* 2004), Sterling (Moore et al. 1993), and from Norton and Smith (1930) as digitized from Jenny (1941). At one of the four sites, AM = Apennine Mountains from (Salciarini *et al.,* 2006), erosion is chiefly a result of landsliding. Data from AM is adjusted by a factor of 54 due mainly to coarser particle size (see Table 1), but to a lesser extent, also a greater infiltration rate. Constant numerical factor applied to data from remaining sites in order to isolate magnitude and shape of soil depth function (values in Table 1 with

1373 discussion in text). Erosion function from Olympic Mountains with original parameters
1374 from Montgomery & Brandon (2002) is used for all sites.

Table 1. Particle size and infiltration rate information across sites

Site[a]	SGM	PL	AM	Sterling	N & S
Climate[b]	Mediterranean	Humid continental	Mediterranean	Semi-arid steppe	NA
P (m/yr)[c]	0.63	1.1	0.9	0.4	NA
I (m/yr)[c]	0.145	0.253	0.207	0.09	NA
x_0 (μm)	30	30	1095	30	NA
Factor[d]	1.00	1.90	54.96	0.58	NA
Ratio[e]	NA	1.60	54.96	1.60	1.50
Percentage[f] (%)	NA	15.8	0	175.9	NA

a. SGM = San Gabriel Mountain, PL = Plastic Lake Basin, AM = Apennine Mountains, N & S = data from Norton & Smith (1930).

b. Climate at SGM, PL, AM and Sterling are referenced from Rulli and Rosso (2005), Buttle and House (1997), Salciarini et al. (2006), and Moore et al. (1993).

c. P is precipitation, I is infiltration. Infiltration rate is estimated as 23% of annual precipitation for each site if run-on and run-off values are not available. I value in SGM is referenced from Yu et al. (2017), precipitation in Plastic Lake is 1.1 m yr^{-1} (Buttle *et al.,* 2004), 0.9 m yr^{-1} for Apennine Mountains (Salciarini *et al.,* 2006), 0.4 m yr^{-1} for Sterling, northeastern Colorado (Moore *et al.,* 1993).

d. Factor used to adapt soil depths calculated as: factor = (particle size on site/30) * (infiltration rate on site/0.145)$^{1.15}$.

e. Ratio necessary to make the data from the 4 sites fit the predicted curve

f. Discrepancy between c) and d) in percent.

Figure 1.

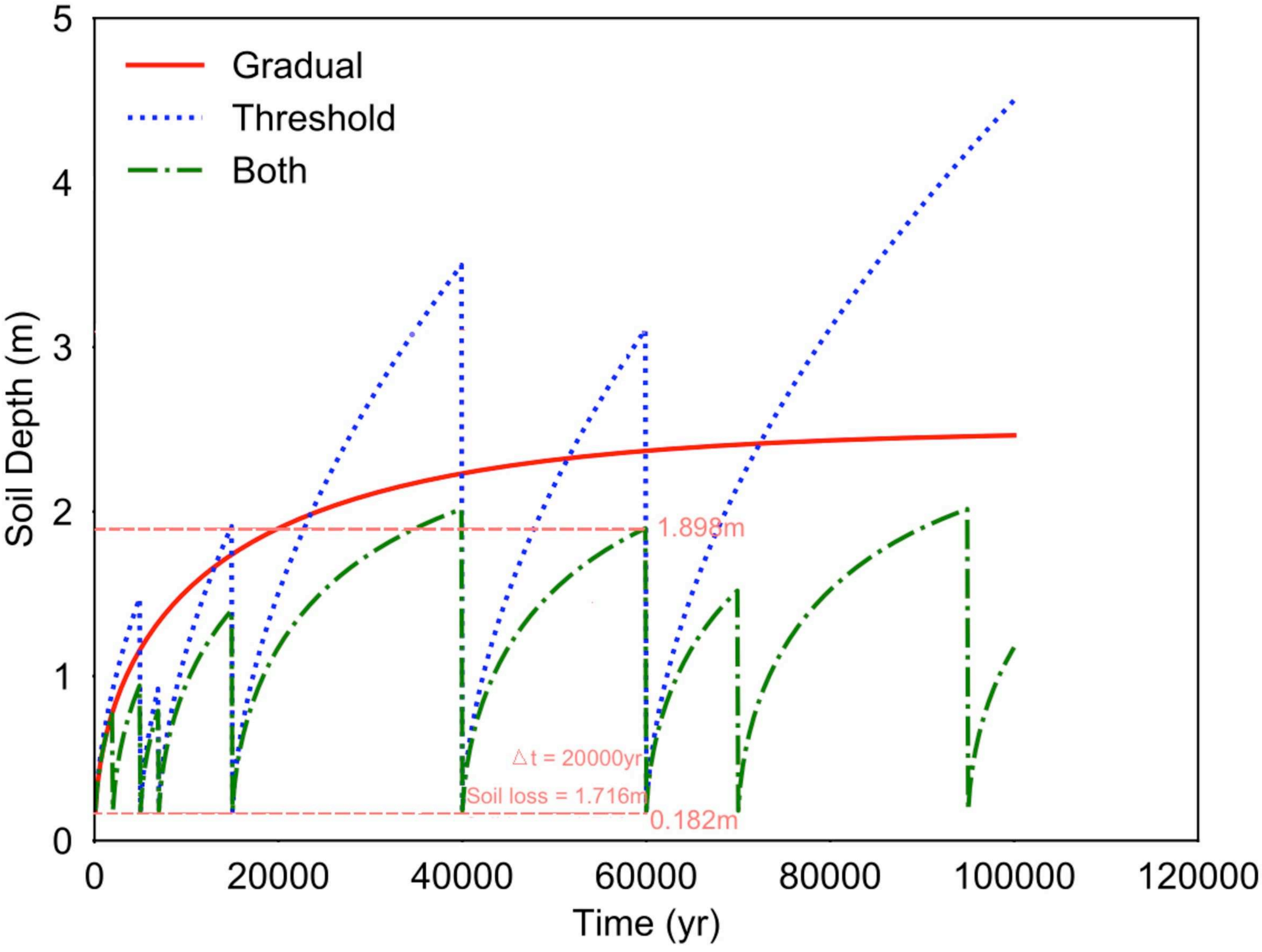
Gradual
Threshold
Both
Soil Depth (m)
Time (yr)
1.898m
0.182m
△t = 20000yr
Soil loss = 1.716m
0
1
2
3
4
5
0
20000
40000
60000
80000
100000
120000

Figure 2.

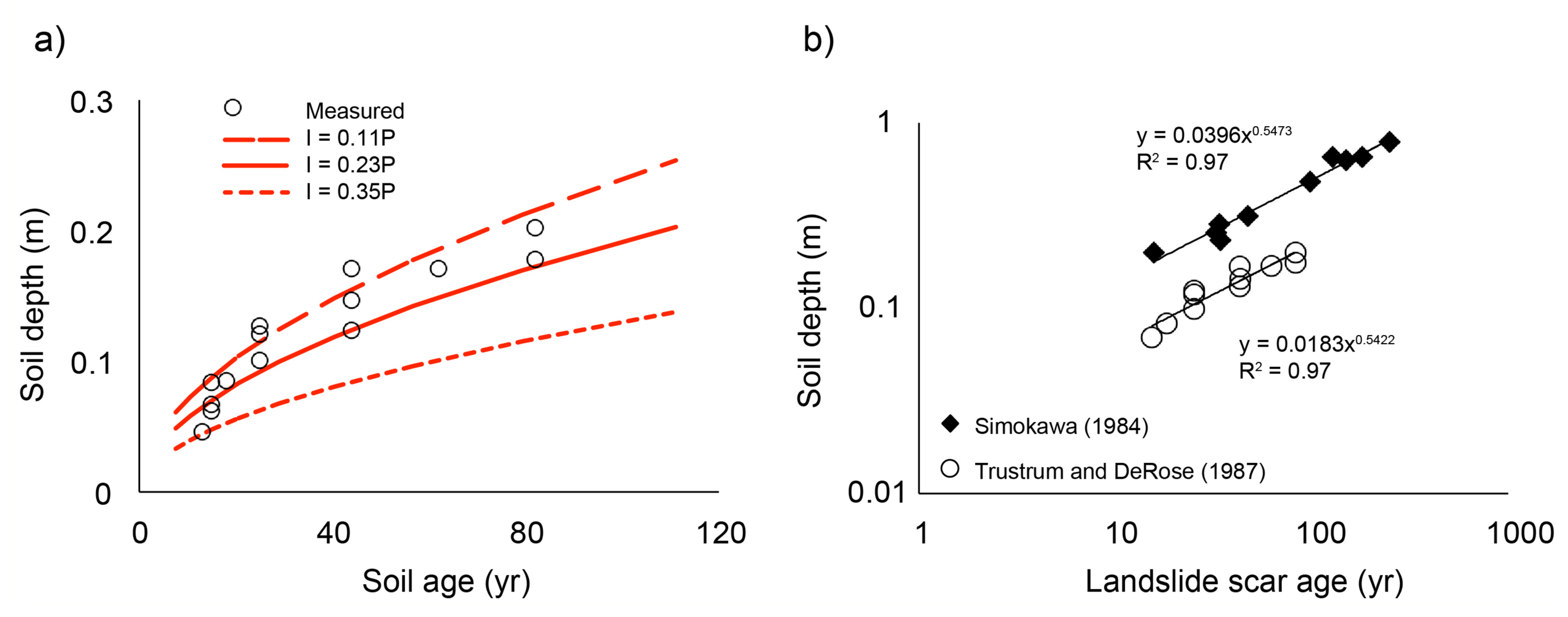
a)
0.3
0.2
0.1
0
Soil depth (m)
Measured
I = 0.11P
I = 0.23P
I = 0.35P
0
40
80
120
Soil age (yr)
b)
1
0.1
0.01
Soil depth (m)
y = 0.0396x^0.5473
R² = 0.97
y = 0.0183x^0.5422
R² = 0.97
Simokawa (1984)
Trustrum and DeRose (1987)
1
10
100
1000
Landslide scar age (yr)

Figure 3.

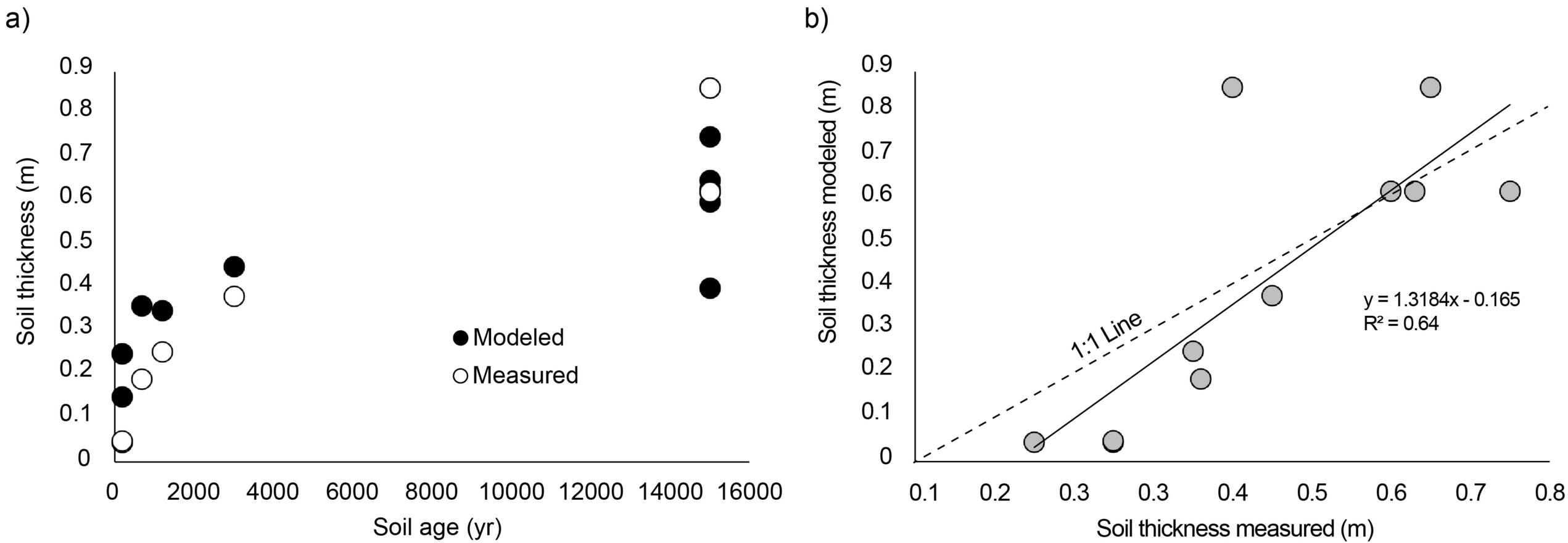
a)
Soil thickness (m)
0
0.1
0.2
0.3
0.4
0.5
0.6
0.7
0.8
0.9
0
2000
4000
6000
8000
10000
12000
14000
16000
Soil age (yr)
Modeled
Measured
b)
Soil thickness modeled (m)
Soil thickness measured (m)
1:1 Line
y = 1.3184x - 0.165
R² = 0.64

Figure 4.

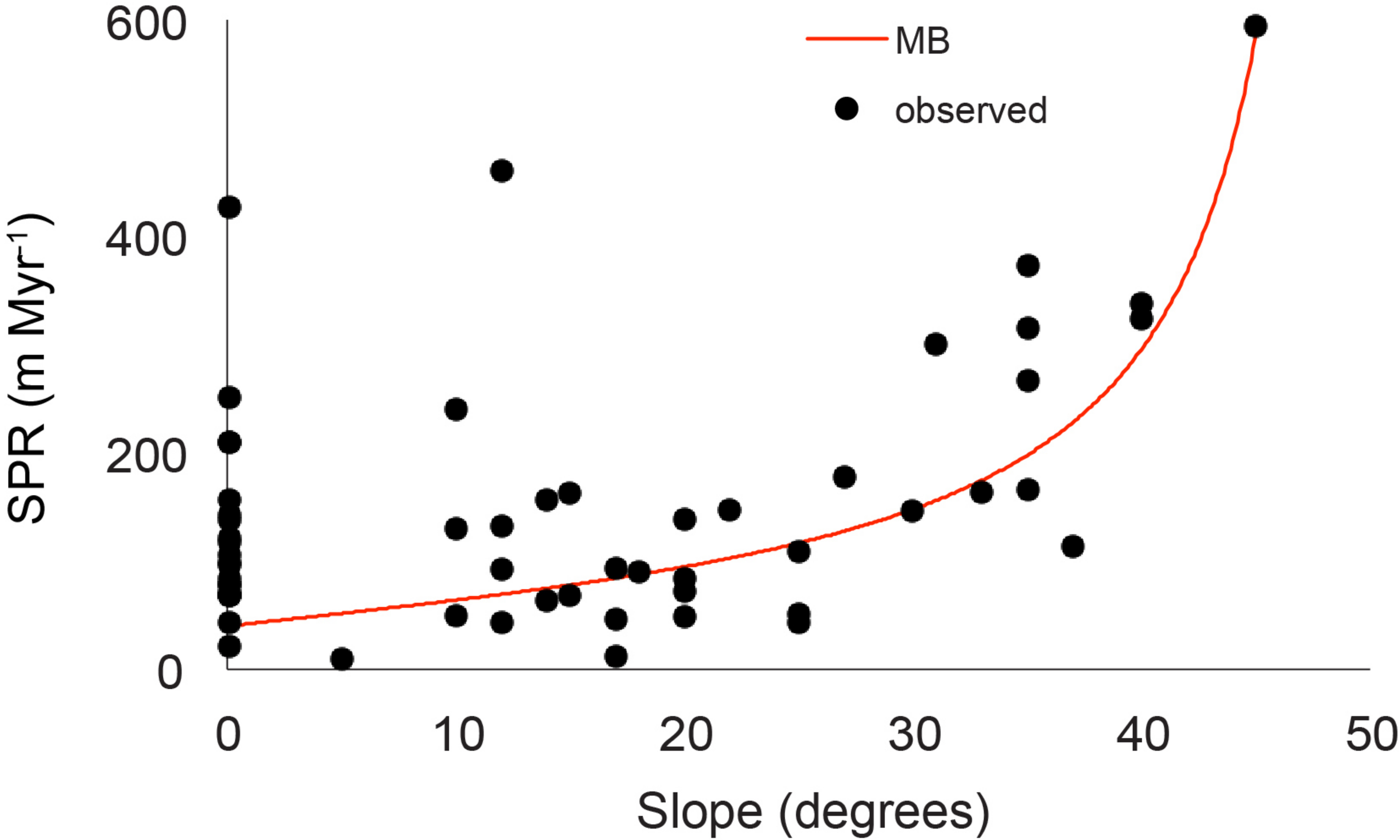
MB
observed
600
400
200
0
SPR (m Myr-1)
0
10
20
30
40
50
Slope (degrees)

Figure 5.

a) Exponential fit

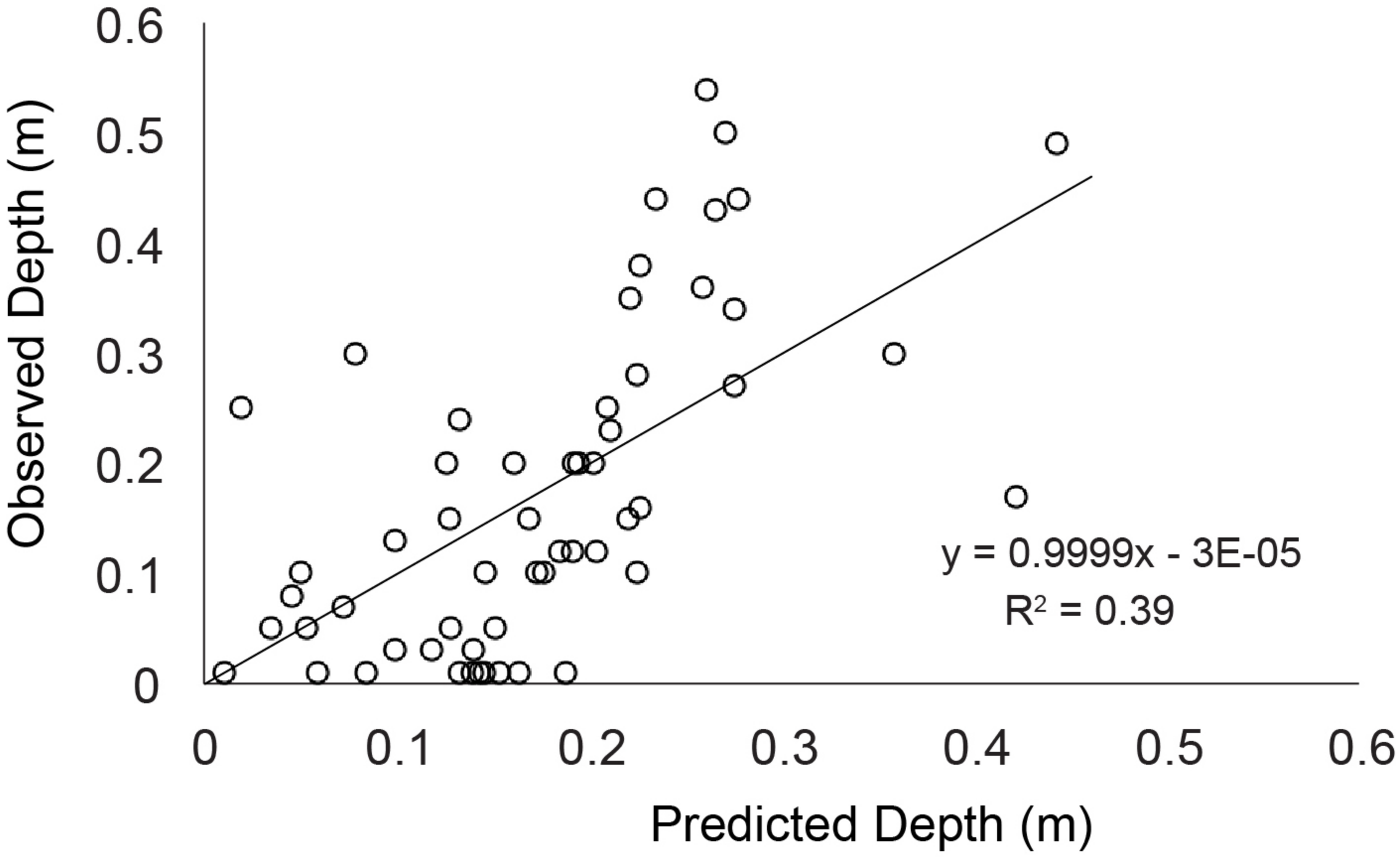

b) Percolation prediction

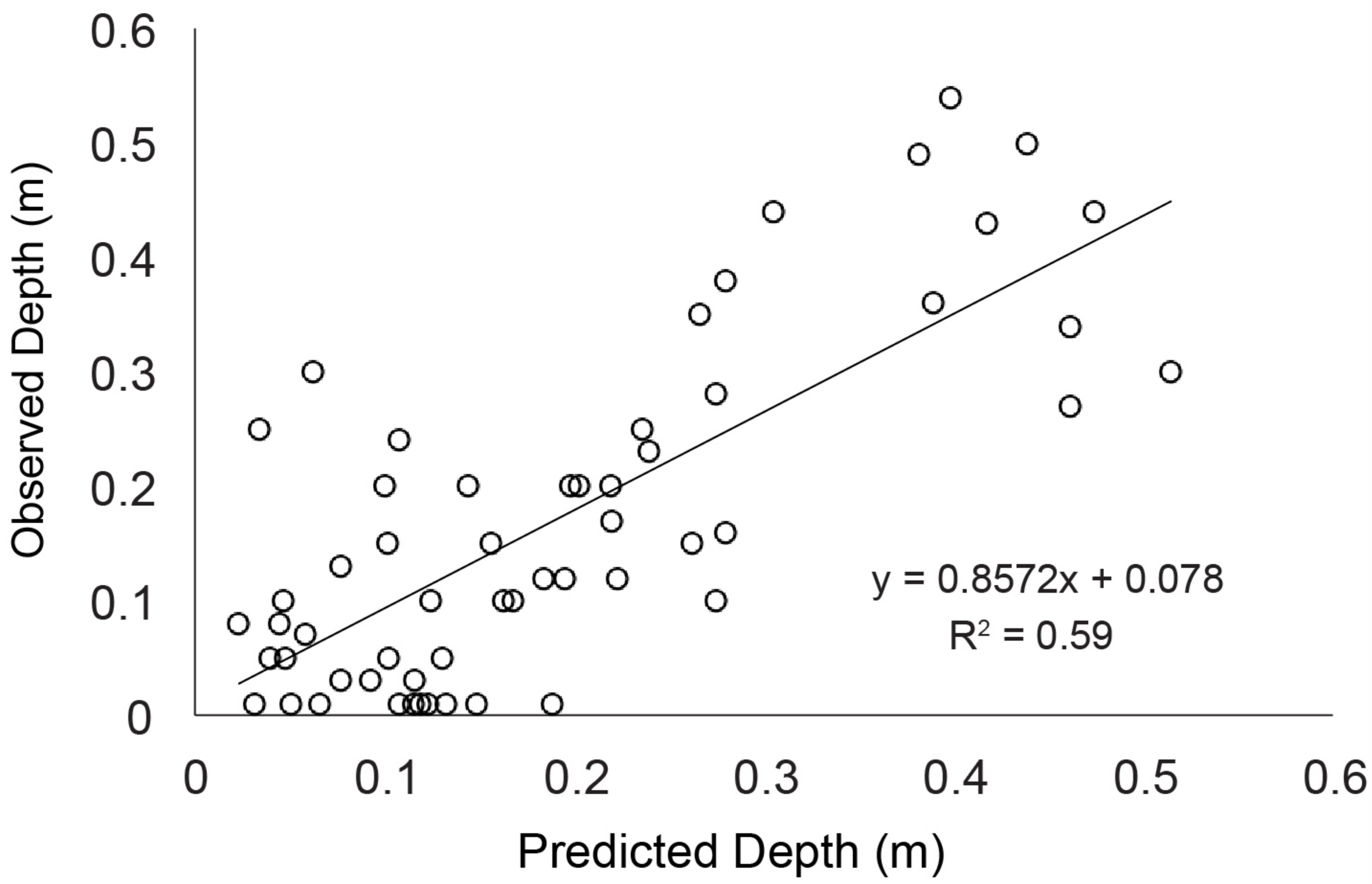

Figure 6.

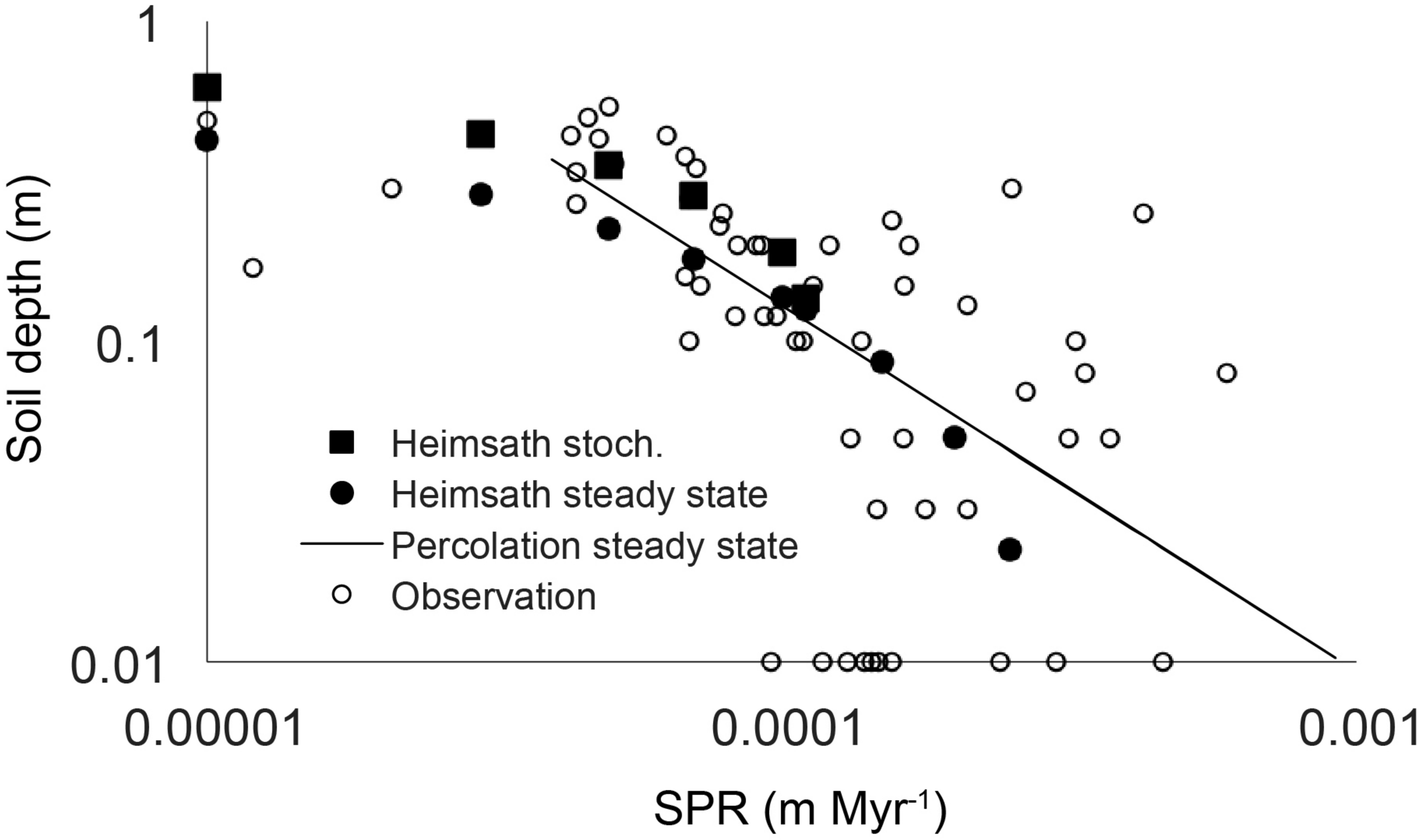
1
0.1
0.01
Soil depth (m)
0.00001
0.0001
0.001
SPR (m Myr-1)
Heimsath stoch.
Heimsath steady state
Percolation steady state
Observation

Figure 7.

a) Exponential fit

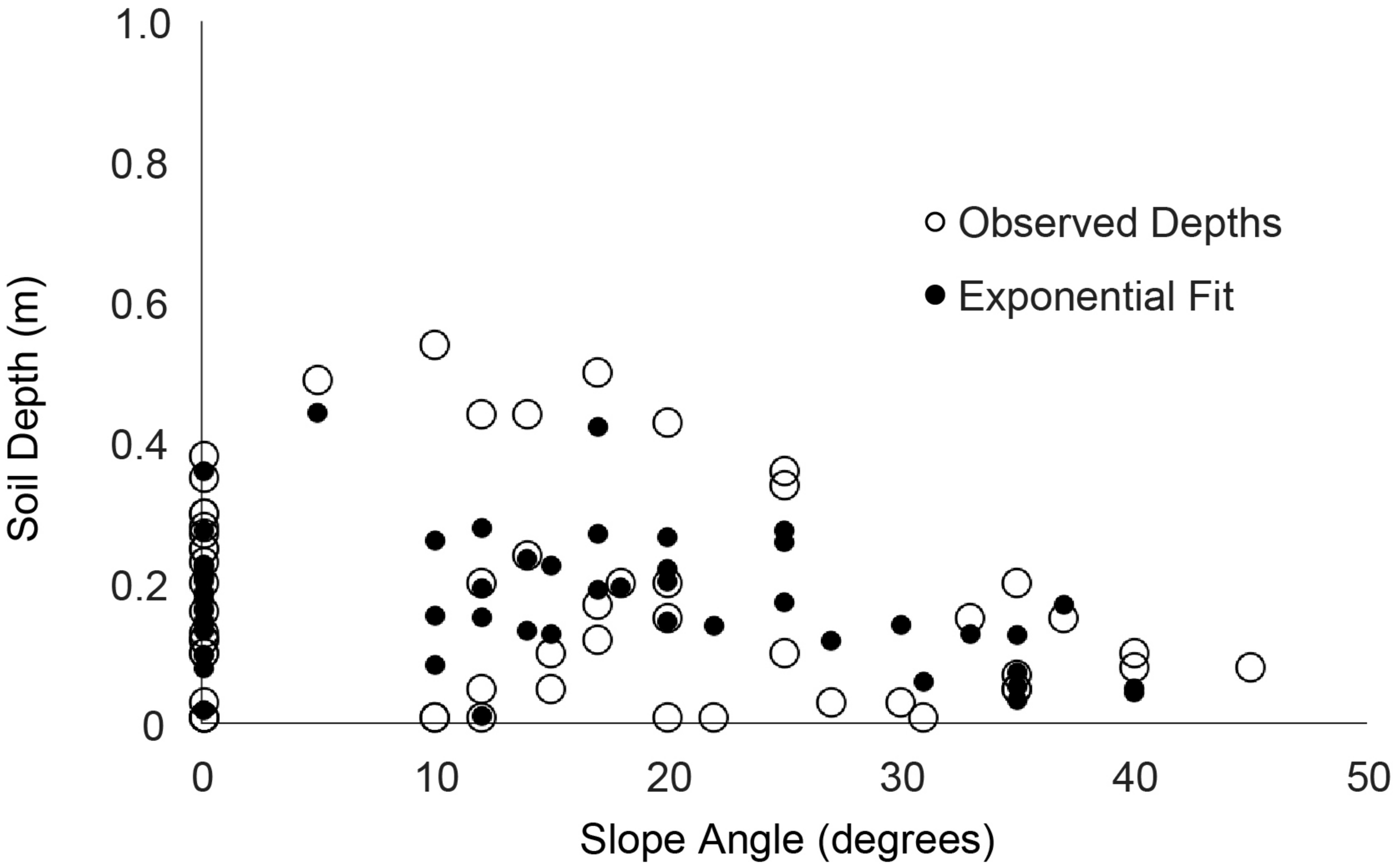

b) Percolation prediction

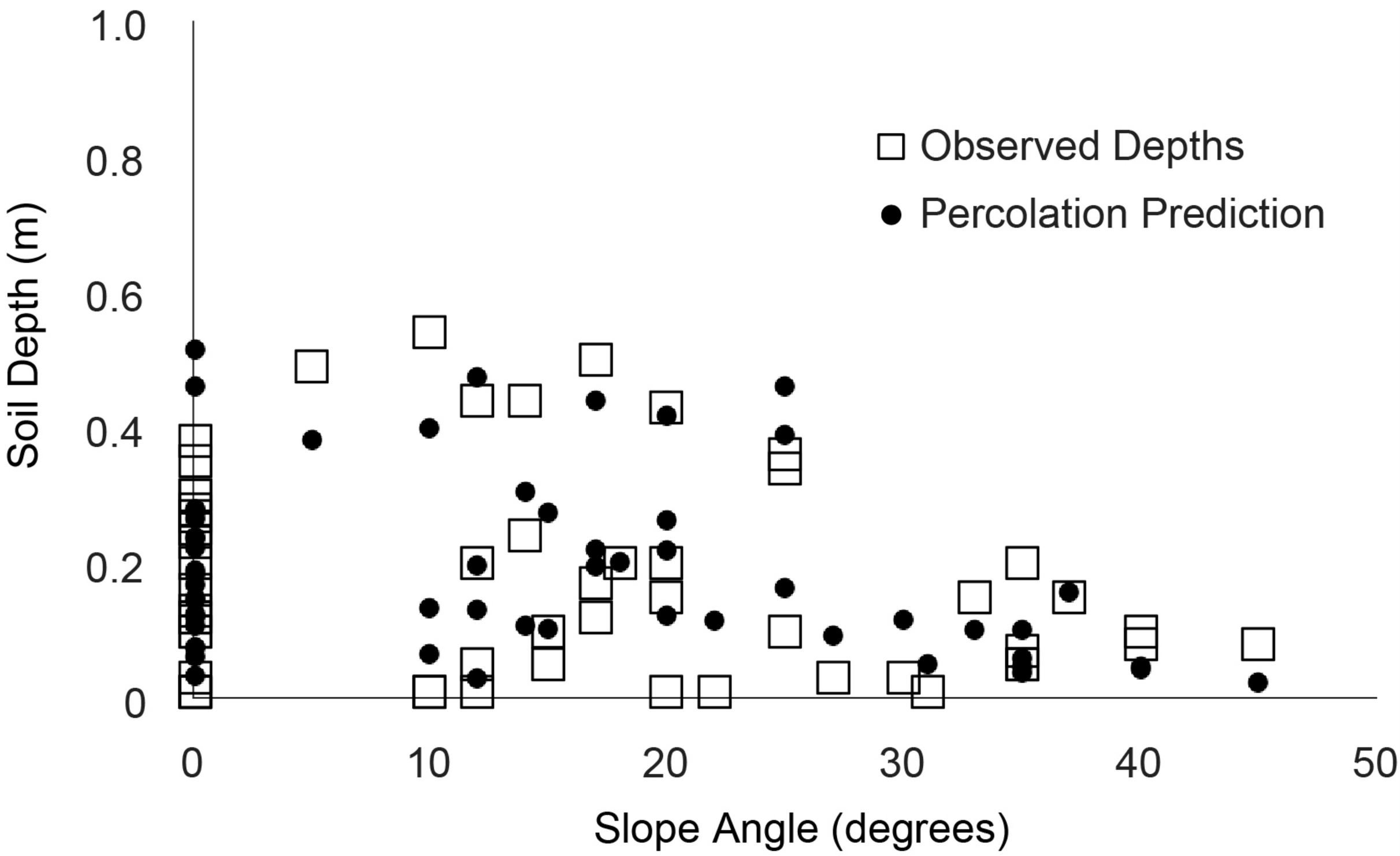

Figure 8.

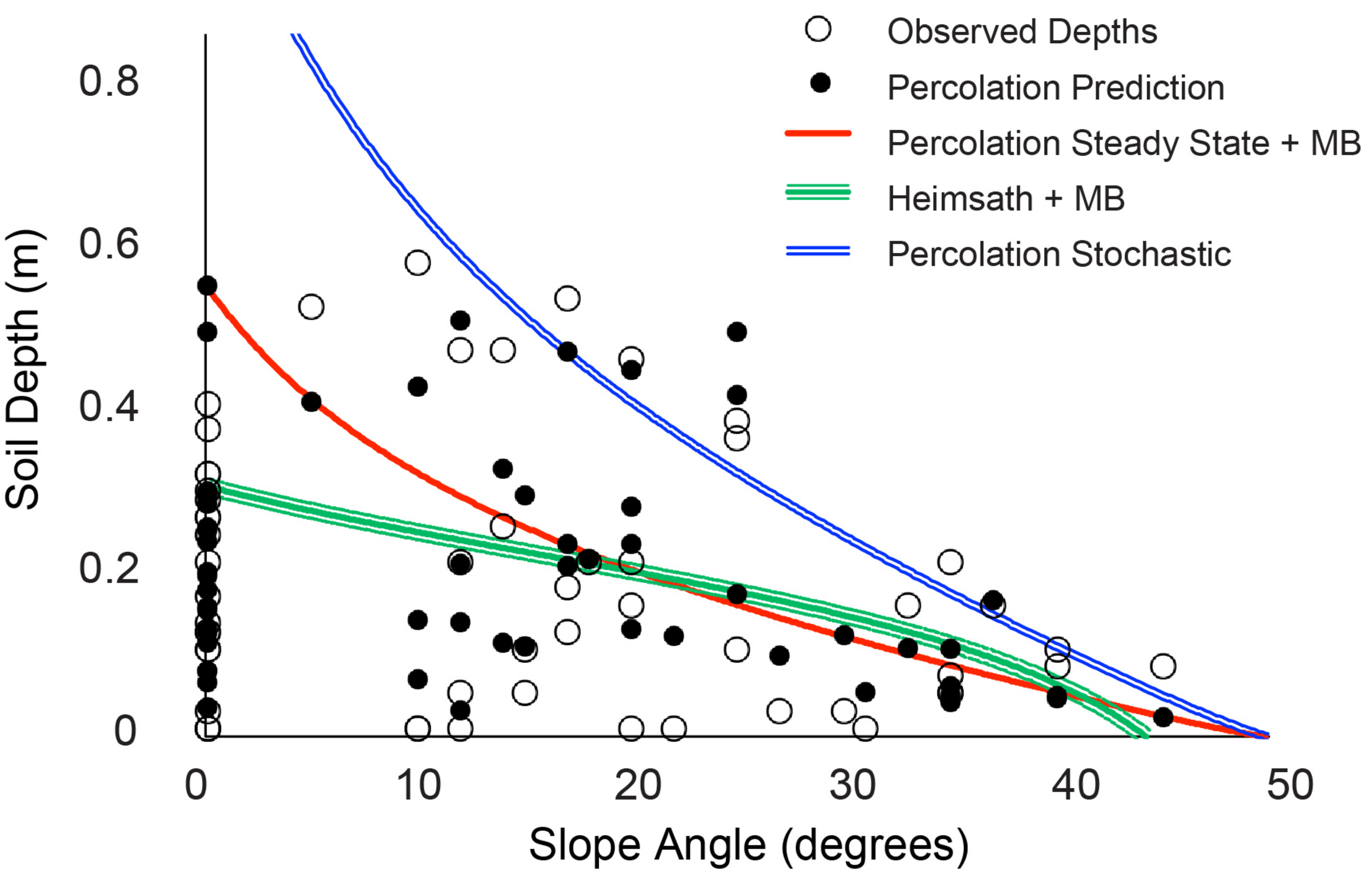
Observed Depths
Percolation Prediction
Percolation Steady State + MB
Heimsath + MB
Percolation Stochastic
Soil Depth (m)
0.8
0.6
0.4
0.2
0
0
10
20
30
40
50
Slope Angle (degrees)

Figure 9.

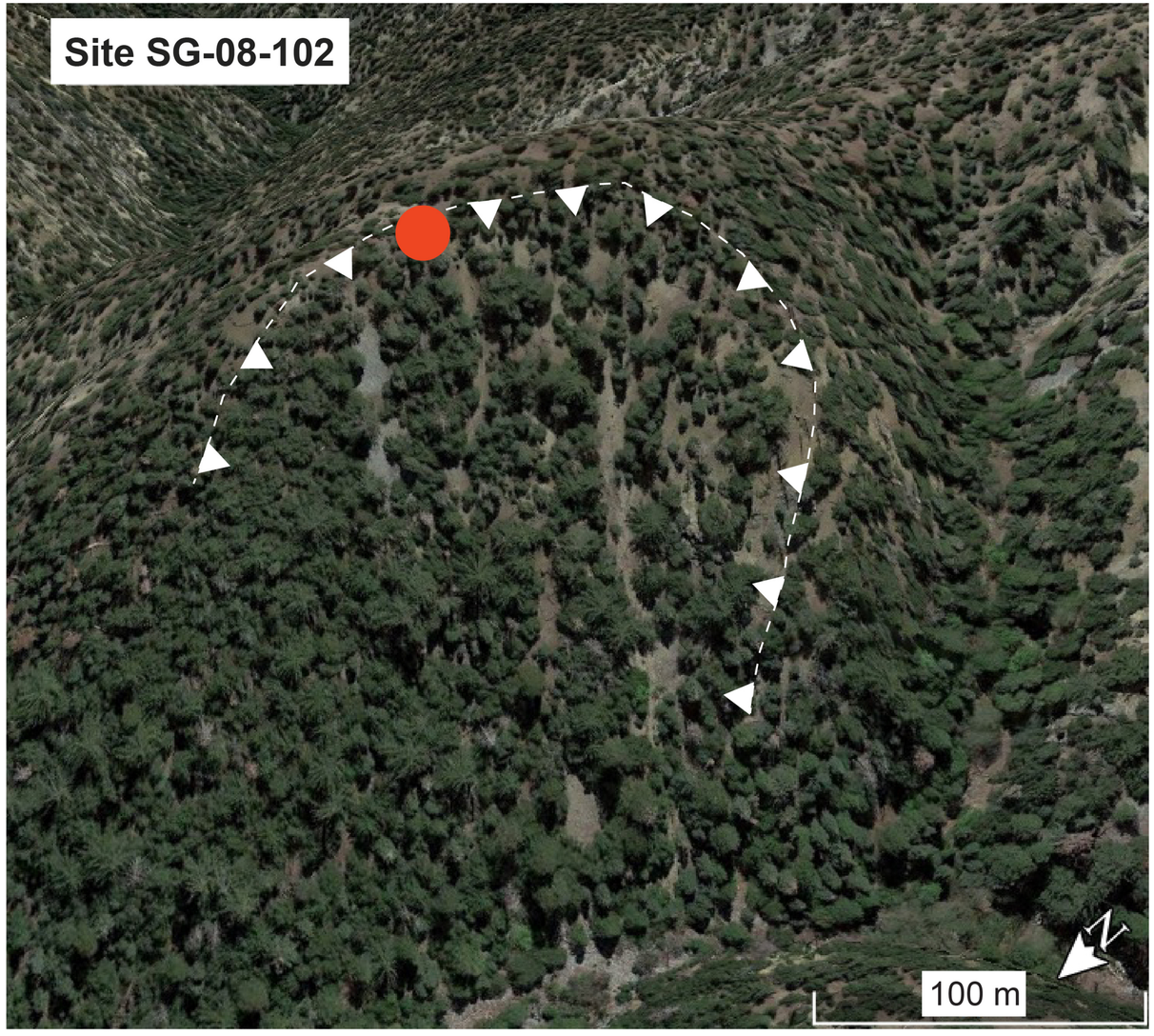
Site SG-08-102
100 m

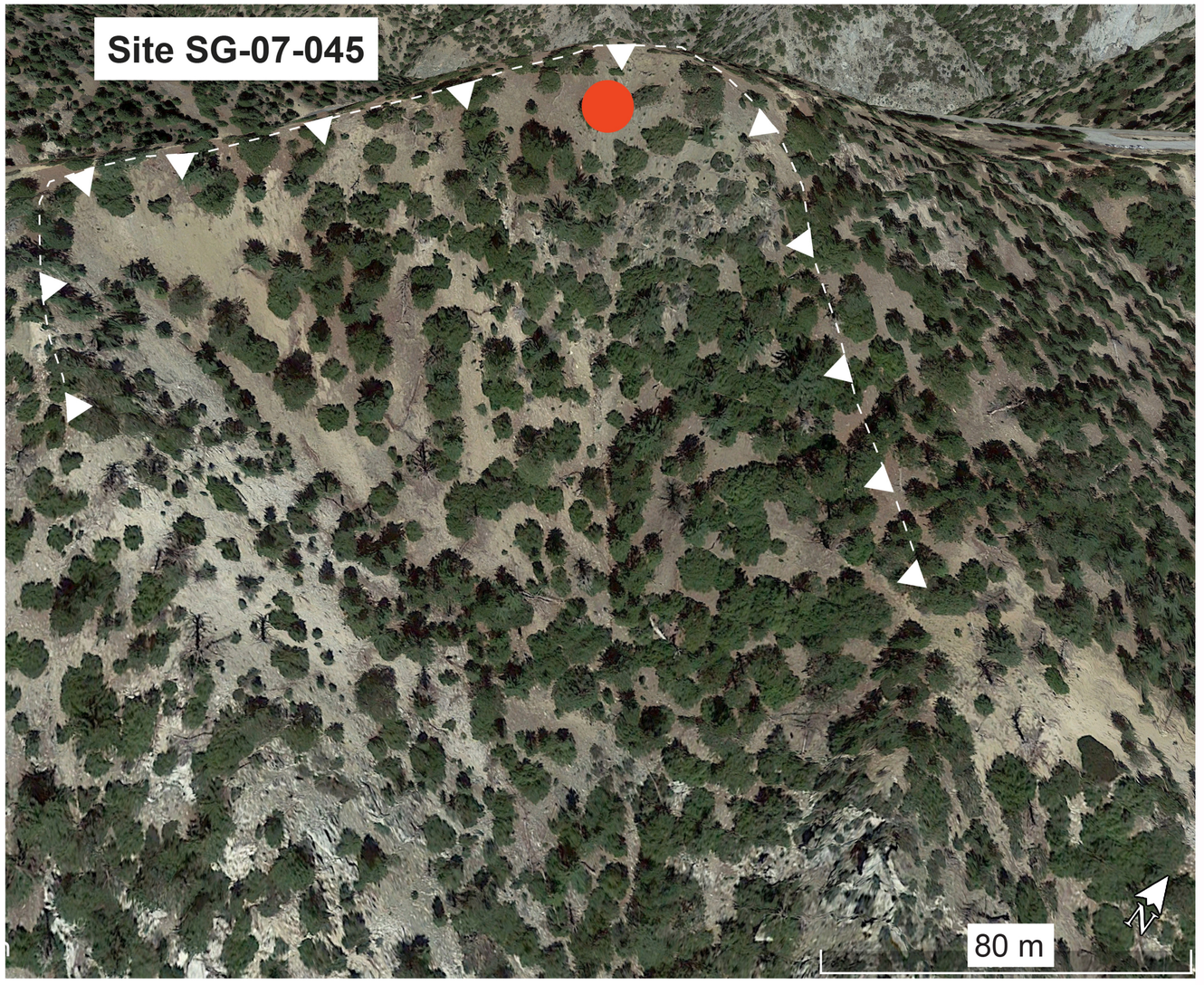
Site SG-07-045
80 m

Figure 10.

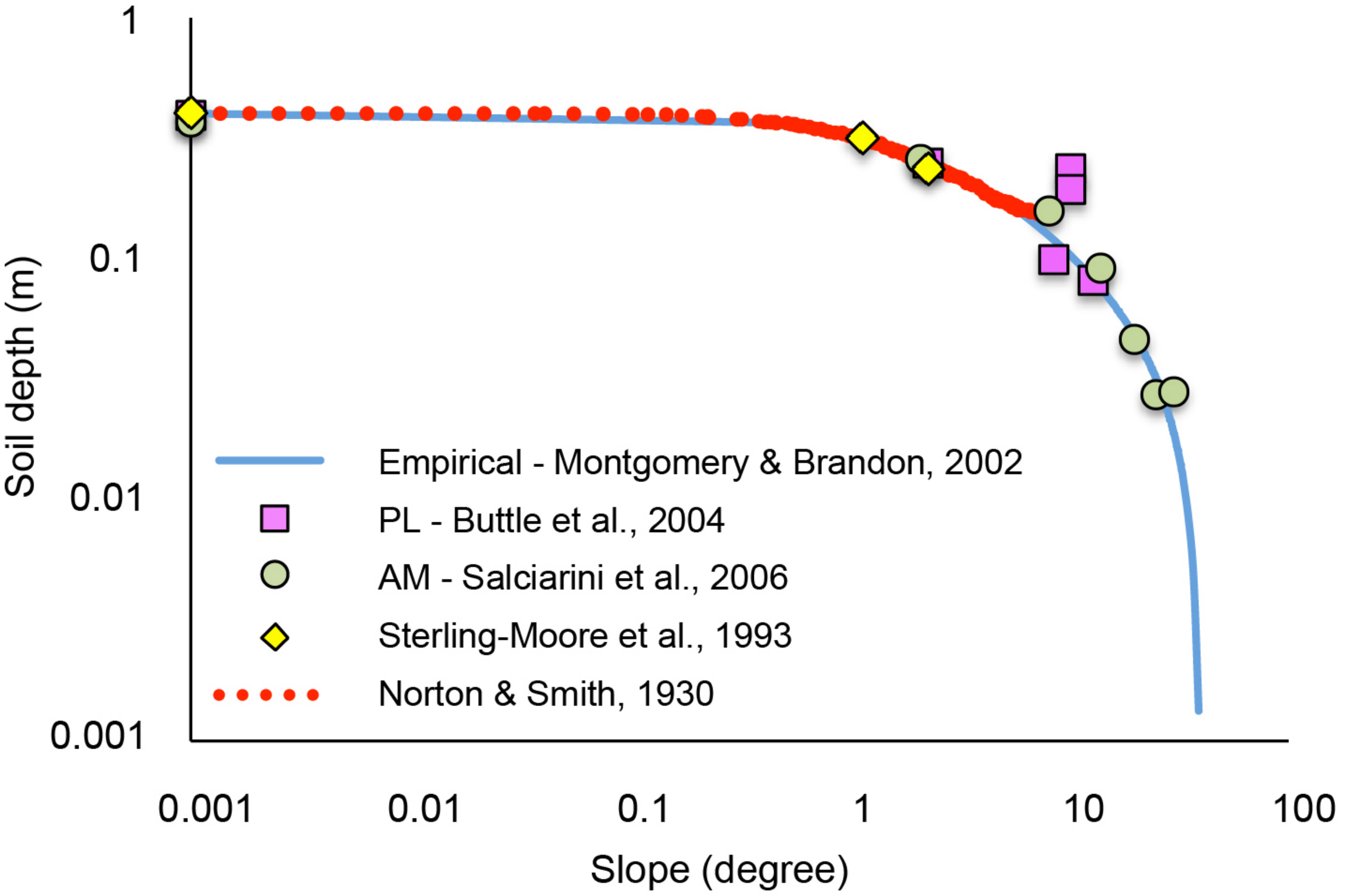
1
0.1
0.01
0.001
Soil depth (m)
0.001
0.01
0.1
1
10
100
Slope (degree)
Empirical - Montgomery & Brandon, 2002
PL - Buttle et al., 2004
AM - Salciarini et al., 2006
Sterling-Moore et al., 1993
Norton & Smith, 1930